Daniel Eduardo Garcia Alvarez

Development of an Optical Force Sensor: A Novel Approach for Monitoring Physical Interaction in Robotic Walkers

Vitória - ES

2026

Daniel Eduardo Garcia Alvarez

Development of an Optical Force Sensor: A Novel Approach for Monitoring Physical Interaction in Robotic Walkers

Dissertation submitted to the Graduate Program in Electrical Engineering from the Technological Center of the Federal University of Espírito Santo, as a partial requirement for obtaining a Master's Degree in Electrical Engineering focused on biomedical engineering and signal processing.

Federal University of Espírito Santo

Technological Center

Graduate Program in Electrical Engineering

Supervisor: Prof. Dr. Camilo Arturo Rodríguez Díaz

Co-supervisor: Prof. Dr. Anselmo Frizera Neto
Prof. Dr. Marcela Cristina Múnera Ramirez

Vitória - ES

2026

Ficha catalográfica disponibilizada pelo Sistema Integrado de Bibliotecas - SIBI/UFES e elaborada pelo autor

---

Garcia Alvarez, Daniel Eduardo, 2001-
G216d Development of an Optical Force Sensor: A Novel Approach for Monitoring Physical Interaction in Robotic Walkers / Daniel Eduardo Garcia Alvarez. - 2026.
73 p.

Orientador: Camilo Arturo Rodriguez Diaz.
Coorientadores: Anselmo Frizera Neto, Marcela Cristina Munera Ramirez.
Dissertação (Mestrado em Engenharia Elétrica) - Universidade Federal do Espírito Santo, Centro Tecnológico.

1. Detectores ópticos. I. Rodriguez Diaz, Camilo Arturo. II. Frizera Neto, Anselmo. III. Munera Ramirez, Marcela Cristina. IV. Universidade Federal do Espírito Santo. Centro Tecnológico. V. Título.

CDU: 621.3

Dissertation approved. Vitória - ES, February 20, 2026:

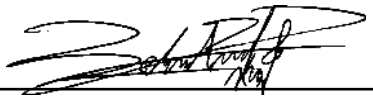

Prof. Dr. Camilo Arturo Rodríguez Díaz
Supervisor
Graduate Program in Electrical Engineering
Federal University of Espírito Santo

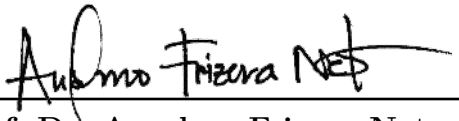

Prof. Dr. Anselmo Frizera Neto
Co-supervisor
Graduate Program in Electrical Engineering
Federal University of Espírito Santo

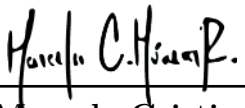

Prof. Dr. Marcela Cristina Múnera Ramirez
Co-supervisor
Bristol Robotics Laboratory
University of the West of England

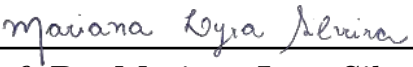

Prof. Dr. Mariana Lyra Silveira
Member of the review board
Graduate Program in Electrical Engineering
Federal University of Espírito Santo

Prof. Dr. Eduardo Rocon de Lima
Member of the review board
Centre for Automation and Robotics
CSIC - Polytechnic University of Madrid

Vitória - ES
2026

Acknowledgements

First, I would like to thank the Universidade Federal do Espírito Santo (UFES) and the Telecommunications Laboratory (LabTel) for giving me the opportunity to pursue my Master's studies. I am also grateful to the funding agencies Coordenação de Aperfeiçoamento de Pessoal de Nível Superior (CAPES); Fundação de Amparo à Pesquisa e Inovação do Espírito Santo (FAPES) (22/2024, 633/2022, 2022-C5K3H, 691/2025, 1336/2025, and 1455/2025); Centro de Pesquisa, Inovação e Desenvolvimento (CPID); Conselho Nacional de Desenvolvimento Científico e Tecnológico (CNPq) (308155/2023-8, 404111/2023-8, 402739/2024-8, and 306323/2024-9); IEEE RAS SPARX; and Petrobras for their support, which made this work possible. I also thank the Bristol Robotics Laboratory, in the United Kingdom, for allowing me to complete a research internship at their facilities, an experience that greatly expanded my academic and professional perspective. On the other hand, I would also like to sincerely thank my supervisor, Camilo Díaz, for welcoming me into his research group and for sharing his knowledge with me. I also thank my co-supervisor, Anselmo Frizera, for his advice and for always being willing to help. I am also thankful to Carlos Cifuentes and Marcela Múnera for believing in me and for supporting my academic and research journey.

Additionally, I would like to emphasize that this work would not have been possible without the support of my family, friends, and colleagues. In particular, I would like to thank my mother, Asseneth Álvarez, for her unconditional support, deep love, and valuable advice. To Lau, for being a great companion during this time and for motivating me every day to be better. To Mafe, for her constant support and for teaching me the value of friendship. To Sergio, who, despite the distance, has always been there to help, and whose conversations and advice have helped me clear my mind. I also thank my Brazilian friends, especially Felipe, Lucas, Isabella, and Henrique, for always making me feel at home. Finally, but not least, I would like to thank my father and angel in heaven, Diego Fernando, whose love, example, and legacy continue to guide my every step. This achievement is yours.

Abstract

This dissertation presents the design, development, and experimental validation of an optical sensor (OS) for monitoring interaction forces in smart walkers (SWs). The proposed sensing approach integrates light-sensitive photodiodes and addressable RGB light-emitting diodes embedded within a compliant encapsulation material, enabling force estimation by measuring changes in optical signals caused by surface deformations. Compared to conventional force-sensing technologies (i.e., strain gauges, piezoelectric sensors, and high-resolution triaxial force cells) and optical fiber-based alternatives (i.e., polymer optical fibers and fiber Bragg gratings), the proposed OS reduces system complexity while offering a cost-effective and easily manufacturable design, facilitating its integration into SWs. The first OS prototype validated the feasibility of the proposed approach, achieving an average force estimation error of 2.4%. Meanwhile, it identified contact zones with an accuracy of 98%. These results demonstrate reliable performance in both force regression and contact localization, as well as the ability to capture the spatial distribution of applied forces. A second development stage focused on a redesigned OS geometry optimized for walker-handle integration, enabling force sensing across multiple interaction zones. An evaluation of the effects of encapsulation materials and illumination wavelengths on OS performance revealed that combination of Ecoflex encapsulation and red light provided the best results, achieving the lowest mean squared error (MSE) (Validation: 4.72 ± 0.31; Test: 4.96), mean absolute error (MAE) (Validation: 1.61 ± 0.04; Test: 1.79), and the highest coefficient of determination (R^2) (Validation: 0.98 ± 0.01; Test: 0.97). The optimized configuration also demonstrated good generalization to unseen loads, with an average error of 5.56%. To assess repeatability, four new OS units implementing the optimized configuration were fabricated and independently calibrated. Among them, the fourth OS achieved the best results, with the lowest prediction errors (MSE validation: 3.11 ± 0.55; test: 3.33; MAE validation: 1.18 ± 0.10; test: 1.24) and the highest correlation values (R^2 validation: 0.98 ± 0.02; test: 0.98). Validation against a commercial reference system confirmed estimation errors below 5.78% across all four OSs. Finally, the integration of the OSs into a SW and their evaluation during path-following trials with ten healthy participants demonstrated consistent force redistribution patterns across straight and turning maneuvers, highlighting the sensor's capability to capture meaningful interaction dynamics in real-world scenarios. Overall, this work demonstrates that waveguide-based OS combined with data-driven models constitutes a robust, scalable, low-complexity, and cost-effective solution for estimating interaction forces in SWs.

Keywords: Robotic Assistive Devices, Smart Walkers, Optical Force Sensor, Feed Forward Neural Network.

Resumo

Esta dissertação apresenta o desenvolvimento e a validação experimental de um sensor óptico (OS, pelas siglas em ingles) para monitorar forças de interação em andadores inteligentes (SWs, pelas siglas em ingles). A abordagem proposta integra fotodiodos sensíveis à luz e LEDs RGB endereçáveis, incorporados em um material de encapsulamento flexível. Dessa forma, a força aplicada é estimada a partir das mudanças nos sinais ópticos causadas pela deformação da superfície. Em comparação com tecnologias tradicionais de medição de força (como extensômetros, sensores piezoelétricos e células de força triaxiais de alta resolução) e com alternativas baseadas em fibras ópticas (como fibras ópticas poliméricas e redes de Bragg em fibra), o OS proposto reduz a complexidade do sistema. Além disso, apresenta um design de baixo custo e fácil fabricação, o que facilita sua integração em SWs. O primeiro protótipo do OS confirmou a viabilidade da proposta, alcançando um erro médio de estimativa de força de 2,4%. Além disso, foi capaz de identificar as zonas de contato com uma precisão de 98%. Esses resultados demonstram um desempenho confiável tanto na estimativa da força quanto na localização do contato, bem como a capacidade de capturar a distribuição espacial das forças aplicadas. Uma segunda etapa de desenvolvimento foi dedicada ao redesenho da geometria do OS, otimizando sua integração ao punho do SW e permitindo a medição de forças em múltiplas zonas de interação. A avaliação dos efeitos do material de encapsulamento e do comprimento de onda da iluminação mostrou que a combinação de encapsulamento em Ecoflex com luz vermelha apresentou os melhores resultados. Essa configuração alcançou os menores valores de erro quadrático médio (MSE) (Validação: 4,72 ± 0,31; Teste: 4,96), erro absoluto médio (MAE) (Validação: 1,61 ± 0,04; Teste: 1,79) e os maiores valores do coeficiente de determinação (R^2) (Validação: 0,98 ± 0,01; Teste: 0,97). A configuração otimizada também demonstrou boa capacidade de generalização para cargas não vistas durante o treinamento, com um erro médio de 5,56%. Para avaliar a repetibilidade, quatro novas unidades do OS, baseadas nessa configuração otimizada, foram fabricadas e calibradas de forma independente. Entre elas, o quarto OS apresentou o melhor desempenho, com os menores erros de predição (MSE validação: 3,11 ± 0,55; teste: 3,33; MAE validação: 1,18 ± 0,10; teste: 1,24) e os maiores valores de correlação (R^2 validação: 0,98 ± 0,02; teste: 0,98). A validação em comparação com um sistema comercial de referência confirmou erros de estimativa inferiores a 5,78% para todos os quatro OS. Por fim, a integração dos OSs em um SW e sua avaliação em testes de seguimento de trajetória com dez participantes saudáveis mostraram padrões consistentes de redistribuição de forças em trajetórias retas e em curvas. Esses resultados destacam a capacidade do sensor de capturar dinâmicas de interação relevantes em cenários reais. De forma geral, este trabalho demonstra que OSs baseados em guias de onda, combinados com modelos orientados por dados, representam

uma solução robusta, escalável, de baixa complexidade e baixo custo para a estimativa de forças de interação em andadores inteligentes.

Palavras-chave: Dispositivos Robóticos Assistivos, Andadores Inteligentes, Sensor Óptico de Força, Rede Neural Feedforward.

List of Figures

List of Tables

List of abbreviations and acronyms

CF	Feedback Capacitor
CP	Cerebral Palsy
DALYs	Disability-adjusted life years
FBG	Fiber Bragg Grating
FNN	Feedforward Neural Network
FSRs	Force-sensing resistors
LC	Load Cells
CSs	Capacitive Sensors
HI	High-income
IMU	Inertial Measurement Unit
LED	Light-Emitting Diode
LMI	Low- and middle-income
LRFs	Laser Range Finders
MAE	Mean Absolute Error
MSE	Mean Squared Error
N	Newtons
OS	Optical Sensor
PD	Photodiode
PLA	Polylactic Acid
POF	Polymer Optical Fiber
RF	Random Forest
Rf	Feedback Resistor
ReLU	Rectified Linear Unit

ROS	Robot Operating System
SAW	Socially Assistive Walker
SCI	Spinal Cord Injury
ST	Stroke
SWs	Smart Walker
WHO	World Health Organization

Contents

1 Introduction

1.1 Motivation

Human gait is a locomotion process in which the body moves forward, alternating support in both lower limbs (VAUGHAN, 2003a). Different musculoskeletal and neurological pathologies considerably affect balance and stability during this process (ECKSTROM et al., 2020). In particular, cerebrovascular accidents or stroke (ST), spinal cord injury (SCI) and cerebral palsy (CP) are commonly found to be strongly related to locomotion impairments, and therefore leading to total or partial loss of mobility and autonomy (BUCHMAN et al., 2011a). Additionally, the progressive deterioration of cognitive functions are related to gait abnormalities (GHENO et al., 2012).

Furthermore, the world is witnessing an unprecedented demographic transformation, with the global population facing a steep rise in aging (United Nations, Department of Economic and Social Affairs, 2020). According to the World Health Organization (WHO), the proportion of individuals over 60 years old is expected to double by 2050, reaching 2.1 billion people (World Health Organization, 2025). Moreover, some clinical findings suggest that coexisting health conditions, such as neurological pathologies, might increase the risk factors of long-term disability and decrease individuals autonomy in activities of daily living (MIKOLAJCZYK et al., 2018).

Considering this, several rehabilitation and assistance devices have been developed to retrain, empower or provide the affected or residual locomotion capacities (KAPSALIS; JAEGER; HALE, 2024). Devices such as canes, crutches, walkers, and wheelchairs, as well as, ambulatory training devices are found in assisted gait and rehabilitation scenarios to improve user's life quality (SIERRA et al., 2019). Regarding conventional walkers, these devices exhibit simple and affordable mechanical structures, as well as, partial body weight support and stability (TODHUNTER-BROWN et al., 2025). However, natural balance, user's energetic costs, fall prevention and security issues are often compromised with conventional walkers (CIFUENTES; MúNERA, 2022). Moreover, several issues related to sensory and cognitive assistance, often required by people with physical limitations, are not completely addressed by conventional devices (MARTINS et al., 2015).

Smart walkers (SWs) have emerged as a promising solution for enhancing mobility, due their simple mechanical design and versatile interaction interfaces (ELANGOVAN; CHANDRAKUMAR; SAKTHIPRIYA, 2025; SIERRA et al., 2024). These devices integrate advanced modules, including autonomous navigation, biomechanical monitoring, safety systems, obstacle avoidance, and user detection strategies, providing comprehensive physi-

cal, cognitive, and sensory support (CIFUENTES et al., 2022a). Among these modules, mechanisms for detecting user movement intentions are crucial in facilitating natural and intuitive interactions during gait (RESCH et al., 2025; VERDEZOTO; BALLESTEROS; URDIALES, 2022; ZOU et al., 2017). These mechanisms enable the walker to interpret the user's physical inputs (typically through sensors located in the handles or base) to dynamically adjust its behavior and provide a better gait experience (CIFUENTES et al., 2022b).

In this context, the development of robust and accessible force-sensing systems emerges as a critical research objetive. These sensors arquitectures must ensure precision, durability, and seamless integration into robotic devices. The combination of cost-effectiveness and technical performance addresses a key challenge: the technological solutions available and their accessibility.

1.2 Objectives

1.2.1 General Objective

To design, develop, and validate an integrated optical sensing architecture for SWs, considering sensor fabrication, electronic interfacing, force estimation using learning-based models, and experimental evaluation of user–device physical interaction.

1.2.2 Specific Objectives

- To design and manufacture an optical sensor (OS), optimizing its configuration for effective integration into SWs.
- To design and implement the electronic interface for conditioning, acquisition, and communication of the optical sensing system.
- To train and implement a feedforward neural network (FNN) to correlate the optical signals with the applied force.
- To evaluate the OS performance under different operating conditions to determine the optimal combination of encapsulation material and illumination wavelength.
- To integrate the optical sensing system into a SW and assess its performance during path-following tasks with healthy subjects.

1.3 Justification

Physical interaction is the main communication channel between the user and the SW, and its accurate measurement is essential for safe assistance (SIERRA et al., 2024; CIFUENTES et al., 2022a). These interaction forces provide information about walking intent, balance, and gait, and their monitoring over time enables the detection of gait changes and potentially unsafe conditions, including an increased risk of falls (SIERRA et al., 2021; ELANGOVAN; CHANDRAKUMAR; SAKTHIPRIYA, 2025; DING et al., 2022). Consequently, accurate and easy-to-implement sensing solutions are essential for SW applications (ZOU et al., 2017).

Traditionally, technologies such as load cells, resistive or capacitive sensors, and high-resolution triaxial cells have been employed for monitoring physical interaction between users and SWs (MARTINS et al., 2015). However, these sensors present significant limitations, including fragility, susceptibility to electromagnetic interference, sensitivity to misalignments, lower compactness, necessity of frequent calibration, and high production costs (LEAL-JUNIOR et al., 2019a). These drawbacks hinder their integration and effective use in SWs, compromising durability and measurement accuracy.

OSs have emerged as alternatives for sensing due to their immunity to electromagnetic interference, flexibility, and compactness (PETERS, 2010). Among the different OSs, optical fiber sensors such as polymer optical fibers (POFs) and fiber Bragg gratings (FBGs) have been the most widely adopted (LEAL-JUNIOR et al., 2019a). POF sensors have been successfully applied to monitor plantar pressure in gait analysis (LEAL-JUNIOR et al., 2019b), measure human-robot interaction forces in exoskeletons (LEAL-JUNIOR et al., 2018), and evaluate spring deflection in series elastic actuators (LEAL-JUNIOR; ANDRADE; FILHO, 2016), offering advantages such as flexibility, biocompatibility, and resistance to electromagnetic interference. Similarly, FBG sensors provide high-precision measurements in distributed sensing applications, including multipoint force monitoring in robotic devices and structural health monitoring of assistive equipment (LEAL-JUNIOR et al., 2019). However, the adoption of FBG technology is restricted by the cost of interrogation equipment (DIAZ et al., 2019; DÍAZ et al., 2018), underscoring the trade-off between sensing capabilities and accessibility (LEAL-JUNIOR et al., 2018).

Furthermore, another scalable and cost-effective solution involves the use of OSs based on waveguide structures (KONSTANTINOVA; STILLI; ALTHOEFER, 2017; LEVI et al., 2013). This approach leverages overlapping signals generated by light emitters and receivers embedded within a waveguide layer (KONSTANTINOVA; STILLI; ALTHOEFER, 2017). When contact deforms the waveguide surface, the internal light propagation is altered, changing the amount of light that reaches the receivers. These variations in optical intensity can then be correlated with the surface deformation and used to accurately estimate the applied force (LEVI et al., 2013). Compared with POF- and FBG-based sensors, this

alternative can simplify system integration and fabrication. In addition, the LEDs can be controlled through a single data line, which helps reduce wiring complexity on the electronic architecture (LEAL-JUNIOR et al., 2019a; PIACENZA et al., 2020). Moreover, these applications have demonstrated the advantage of data-driven methods over analytical models, enabling the automatic extraction of complex features and patterns (PIACENZA et al., 2020). In particular, analytical models typically require the underlying physical relationships to be explicitly formulated in advance, which becomes challenging when the sensor response depends on multiple coupled variables and non-uniform deformation effects (PIACENZA et al., 2020). Although this technology has great potential, integration into SWs has not been extensively studied in existing literature.

In this sense, the main proposal of this work is the validation of a sensor based on this novel concept involving OSs. Furthermore, how with a data-driven deep learning method it is possible to accurately estimate the applied force. Thus, a fully integrated sensor will be presented that uses affordable fabrication methods for easy integration into SWs, improving functionality, accuracy and reducing complexity and fabrication costs.

1.4 Contributions

Design and fabrication of a novel optical force sensor: This work introduced an optical sensing architecture based on overlapping light emitter–receiver embedded in a silicone waveguide. To the best of the author knowledge, no prior studies had implemented this sensing concept in SWs. The proposed design provided a compact, low-cost, and mechanically compliant solution suitable for integration into these assistive devices.

Experimental analysis of encapsulation materials and illumination wavelengths: An evaluation of two encapsulation materials and multiple light-emitting diode (LED) wavelengths was conducted to characterize light transport, and signal stability. This analysis identified the optimal material–wavelength configuration for maximizing force measurability while ensuring robustness and manufacturability.

Development of data-driven models for force estimation: This dissertation implemented and trained FNN architectures to estimate the applied force from the photodiode (PD) signals, achieving high prediction accuracy. These models demonstrated the suitability of deep learning for interpreting complex deformation patterns.

Integration of the OS in a SW and validation with healthy participants: Four sensing units were mounted into the handlebar of the socially assistive walker of the Bristol Robotics Laboratory to monitor user–device interaction. The system was validated through controlled experiments and walking trials with healthy participants, demonstrating its ability to capture gripping, unloading, and turning-related force patterns in real conditions. This constituted one of the first integrations of optical waveguide-based

sensors into SWs.

1.5 Publications

1. (Conference Proceedings) **Garcia A., Daniel E.**; et al. (2025). "Development of an Optical Technology-Based Sensor and Deep Learning Models to Estimate User-Interaction Forces in Smart Walkers". In: **Proc. SPIE 13313, Biophotonics in Exercise Science, Sports Medicine, Health Monitoring Technologies, and Wearables VI**. DOI: 10.1117/12.3043576. (Oral presentation)

2. (Journal Article) **Garcia A., Daniel E.**; et al. (2025). "Optical Force Sensor for Walker-Assisted Navigation". In: **IEEE Transactions on Instrumentation and Measurement (TIM)**. (Manuscript in progress)

1.6 Document Organization

This master's dissertation presents the development and validation of an OS designed to estimate user–walker interaction forces. The document is organized into five chapters, progressing from the motivation and background to the design, evaluation, and final discussion of the proposed system. The document is structured as follows:

Chapter 1 introduces the general context and motivation for this work, defines the research objectives, and presents the justification for the proposed study. It also summarizes the main contributions of the dissertation, lists the resulting publications, and provides an overview of the document organization.

Chapter 2 reviews existing technologies for measuring interaction forces in assistive devices. It discusses the limitations of conventional sensing approaches and introduces optical alternatives (such as POF, FBG, and optical waveguide-based sensors) that motivate the proposed solution.

Chapter 3 details the design, fabrication, and calibration of the proposed OSs. It presents the two sensor versions, the selection of encapsulation materials and LED wavelengths, the data acquisition process, and the learning algorithms used for force estimation. The chapter also describes the integration of the sensors into a SW and the experimental protocols.

Chapter 4 reports the experimental results for both sensor versions, including PD responses, force estimation performance, material–wavelength comparisons, and multi-point indentation tests. It also presents the validation against a commercial reference system and the outcomes of the walking trials with healthy participants.

Chapter 5 summarizes the main conclusions and contributions of the study by revisiting the most relevant findings obtained throughout the design, fabrication, validation, and application stages of the proposed sensor. It also emphasizes the practical relevance of the device for force measurement in smart rollator systems and discusses several directions for future research, including possible improvements in sensor design, signal processing, and experimental evaluation.

2 State of Art

This chapter provides a general overview of the challenges that affect human mobility and introduces the assistive devices commonly used to support individuals with mobility limitations, with particular emphasis on the impact of SWs. It also reviews the sensing technologies used to measure interaction forces between users and these devices, as these forces provide important information about user support and behavior during gait. Thus, the chapter first examines traditional sensors and then presents optical sensing approaches designed to overcome the limitations of conventional methods. Finally, it identifies the gaps in current research that motivate the development of the OS proposed in this dissertation, establishing the foundation for the design and evaluation presented in the following chapters.

2.1 Human Gait and Mobility Challenges

Human gait is a cyclic and bipedal pattern that allows forward movement through the coordinated actions of the lower limbs and the trunk (VAUGHAN, 2003a). This process involves a sequence of movements in which one leg provides support while the other advances, creating a continuous and rhythmic progression (ADOLPH et al., 2012). It also relies on the effective interaction between the musculoskeletal system, which is responsible for force generation and joint motion, and the nervous system, which regulates timing, coordination, and balance (VAUGHAN, 2003b; DECKER; CIGNETTI; STERGIOU, 2010). When these systems function properly, gait is stable, efficient, and adaptable (DECKER; CIGNETTI; STERGIOU, 2010; BUCHMAN et al., 2011b). However, it can be affected by different neurological, musculoskeletal, and age-related conditions that often reduce the individual's ability to walk safely and independently (CICIRELLI et al., 2021). Among these conditions, ST, SCI, and CP are strongly associated with cognitive decline, impaired motor control, and the partial or total loss of locomotor abilities (CIFUENTES; FRIZERA, 2016; SIERRA et al., 2021).

Regarding ST, global reports show that cerebrovascular accidents are the second leading cause of death and the third main cause of long-term disability in adults (FEIGIN et al., 2025). According to the WHO, nearly 15 million people suffer a ST each year worldwide (World Health Organization, 2024c). Of these cases, about 5 million result in death and another 5 million lead to permanent disability (JOHNSON; NGUYEN, 2019). A systematic review also reported a 42% decrease in ST incidence in high-income (HI) countries (JOHNSON et al., 2016). However, during the same period, the incidence in low- and middle-income (LMI) countries more than doubled (FEIGIN; KRISHNAMURTHI,

2014; JOHNSON et al., 2016). In line with this trend, some findings indicated that 85.5% of global ST-related deaths occurred in LMI countries (FEIGIN et al., 2025). The same report showed that disability-adjusted life years in these regions were nearly seven times higher than in HI countries.

Additionally, SCI represents another cause of long-term disability worldwide, affecting both motor function and sensory processing (Mayo Clinic, 2019; HU et al., 2023). According to the WHO, 15 million people live with this condition, and between 250,000 and 500,000 new cases occur each year (World Health Organization, 2024b). An epidemiological study indicates that the number of affected individuals doubled between 2003 and 2011 (YANG et al., 2014). Global statistics report an annual incidence of 40 to 80 cases per million people, with nearly 90% of these injuries resulting from traumatic events such as road traffic accidents and falls (LU et al., 2024; World Health Organization, 2024b; Mayo Clinic, 2019). Furthermore, studies show that approximately 80% of new cases occur in males, and individuals between 16 and 30 years old are at the highest risk of sustaining a traumatic SCI (AMIDEI et al., 2022).

Similarly, CP constitutes another major cause of motor impairment, characterized by non-progressive disturbances in movement and posture resulting from early brain injury (RICHARDS; MALOUIN, 2013; VITRIKAS; DALTON; BREISH, 2020). These affectations are often accompanied by deficits in sensation, perception, cognition, communication, and behavior (VITRIKAS; DALTON; BREISH, 2020; PAUL et al., 2022). According to worldwide reports, its prevalence ranges from 1.5 to 4 cases per 1,000 live births or children of a similar age range (STAVSKY et al., 2017). In addition, available evidence suggest that approximately 764,000 people live with CP, of whom around 500,000 are children and adolescents (Mimi Poinsett, 2019). Spastic CP is the most common form, accounting for nearly 80% of all diagnosed cases (PAUL et al., 2022).

Finally, it is important to highlight that with aging, a wide range of health conditions progressively affects individuals' well-being and functional autonomy (BROWN; FLOOD, 2013). More than half of adults over 65 live with three or more chronic conditions, including cardiovascular disease, hormonal changes, and musculoskeletal disorders. Mobility and balance are compromised due to gradual declines in the nervous, musculoskeletal, and cardiorespiratory systems (ECKSTROM et al., 2020; NABILI; DAVIS, 2019). Gait alterations are also frequent, as older adults walk more slowly, take shorter steps, and adopt a wider stance to maintain stability (ROHOR et al., 2025; PIRKER; KATZENSCHLAGER, 2017). In addition, epidemiological studies indicate that gait and balance problems become more prevalent with age (ROHOR et al., 2025), increasing from approximately 10% in people aged 60–69 to over 60% in those over 80 (World Health Organization, 2025; MIKOLAJCZYK et al., 2018). At the same time, the global population is aging rapidly (United Nations, Department of Economic and Social Affairs, 2020). By 2020, the number

of people over 60 surpassed the population of children under 5, and by 2050, this group is expected to double from 900 million to more than 2 billion, with nearly 80% living in LMI countries (World Health Organization, 2025).

2.2 Mobility Assistive Devices

Mobility limitations caused by neurological, musculoskeletal, and age-related conditions often require external support to assist individuals with reduced gait stability or impaired motor control (CIFUENTES et al., 2022a; ATOYEBI et al., 2019). Consequently, a wide range of mobility assistive devices has been developed to enhance safety and promote functional independence (CIFUENTES; MúNERA, 2022). These devices range from simple mechanical aids (such as canes, crutches, treadmills, and wheelchairs) to more advanced robotic systems that integrate multiple sensors and actuators to provide more effective and responsive assistance, such as SWs (GARCIA et al., 2021; MARTINS et al., 2015). Each device offers different levels of stability, weight support, and gait assistance depending on the user's functional capacity.

2.2.1 Conventional Approaches

Conventional assistive technologies rely on simple mechanical structures to provide stability, support weight transfer, and facilitate gait initiation (COWAN et al., 2012). Despite their limited adaptability, they have been implemented due to their low cost, easy operation, and well-established clinical benefits (KAPSALIS; JAEGER; HALE, 2024). These devices are also integrated into therapeutic programs to promote balance recovery, enhance postural control, and facilitate the safe practice of basic locomotor tasks (TODHUNTER-BROWN et al., 2025). Their simplicity ensures reliable operation in both clinical and daily environments, without the need for sensing or actuation components (World Health Organization, 2024a).

In daily living environments, canes and walking sticks serve as basic aids for individuals who need extra stability or help when shifting their weight (LEE et al., 2021). Quad-canes are often prescribed when greater stability is required, as they provide four points of contact with the ground (AERKEN; CLARK; BRODERICK, 2024). Crutches are typically used after orthopedic injuries and allow partial or full weight support while relying on the strength of the upper limbs. Forearm crutches offer an additional advantage because the cuff supports the forearm and keeps the crutch properly aligned, allowing the hands to be briefly free for simple tasks (RASOULI; REED, 2020). This design makes them more comfortable and practical for long-term use.

Additionally, wheelchairs are the most common solution for individuals who are unable to walk independently, offering full-body support and mobility through user or

caregiver propulsion (World Health Organization, 2023). Parallel bars are frequently used in rehabilitation to train balance, strengthen lower limbs, and support early standing or stepping exercises in a controlled environment (SIERRA et al., 2019). In addition, treadmill-based systems provide repetitive gait practice, and when combined with body-weight support harnesses, they allow individuals with severe instability or limited postural control to train safely (ALASHRAM; ANNINO; PADUA, 2021; SCHMITT et al., 2021). These tools are essential during early rehabilitation phases, as they help patients regain confidence and rebuild fundamental gait components.

However, as mobility demands increase, some individuals require devices that offer greater support than canes or crutches (MARTINS et al., 2015). Walking frames, or walkers, provide greater support by offering a stable structure that enhances balance and allows partial weight bearing (ELANGOVAN; CHANDRAKUMAR; SAKTHIPRIYA, 2025). Their simple mechanical design enables users to engage their remaining locomotor abilities while receiving external support during standing and gait initiation (POSTOLACHE et al., 2015). Standard walkers, consisting of a rigid four-legged frame with rubber tips, provide high stability but require users to lift and advance the device at each step, often resulting in slower and less natural gait patterns and demanding sufficient upper-body strength and cognitive capacity (ELANGOVAN; CHANDRAKUMAR; SAKTHIPRIYA, 2025; POSTOLACHE et al., 2015). Front-wheeled walkers incorporate two wheels on the front legs, eliminating the need to lift the device and making them more suitable for users with limited upper-limb strength. This configuration facilitates smoother forward movement and allows for more natural gait patterns and increased walking speed (PHAM; DUONG; SUH, 2017).

However, despite their widespread use, conventional assistive devices often increase the user's energetic cost, and offer limited support for fall prevention and safety (CIFUENTES; MúNERA, 2022). Moreover, sensory and cognitive assistance requirements, which are frequently needed by individuals with physical impairments, are not fully addressed by these devices (MARTINS et al., 2015).

2.2.2 Robot-Assisted Alternatives

Advances in sensing, actuation, and control technologies have led to the development of robotic mobility aids that provide more adaptive and responsive assistance than conventional devices (CIFUENTES; MúNERA, 2022). These systems support users during walking by offering controlled guidance, monitoring movement in real time, and adjusting assistance according to individual needs (CHAPARRO-CÁRDENAS et al., 2018). Depending on the level of mobility impairment, robotic devices can provide full support (such as robotic wheelchairs or autonomous mobility platforms) or complement the user's remaining abilities through powered gait trainers, body-weight support systems, or wearable systems

(CIFUENTES; FRIZERA, 2016; MARTINS et al., 2012). This technological progress has also enabled the emergence of SWs (FRIZERA-NETO et al., 2015b), which extend traditional walker capabilities by integrating sensing and advanced control modules to provide more effective physical, cognitive, and sensory support during gait (ELANGOVAN; CHANDRAKUMAR; SAKTHIPRIYA, 2025). Figure 1 shows some SWs presented in the literature.

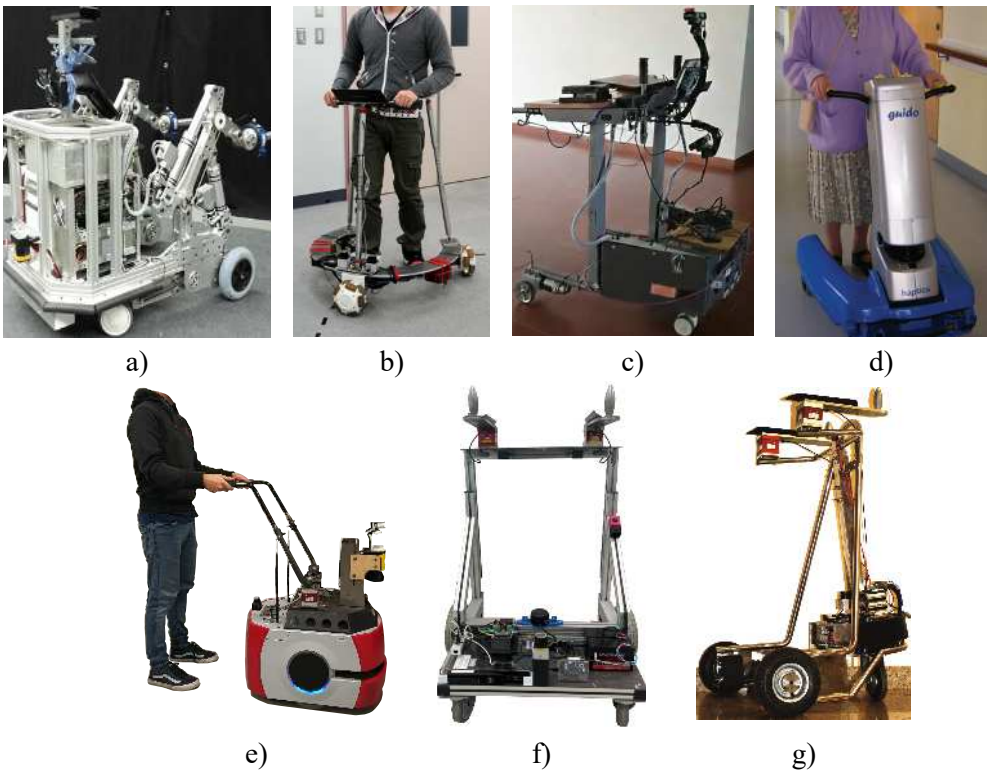

Figure 1 – SWs reported in the literature. a) MOBOT (GERAVAND et al., 2016a). b) JARoW (OHNUMA; LEE; CHONG, 2011). c) WALKit (GONÇALVES et al., 2023). d) GUIDO (LACEY; RODRIGUEZ-LOSADA, 2008). e) AGoRA (SIERRA et al., 2019). f) UFES vWalker (MACHADO et al., 2024). g) UFES walker (FRIZERA-NETO et al., 2015a).

Many SWs incorporate multiple sensing modules to better perceive both the environment and the user, enabling safer and more intuitive assistance during gait (FRIZERA-NETO et al., 2015b). Early platforms such as GUIDO (LACEY; RODRIGUEZ-LOSADA, 2008) and the XR4000 (MORRIS et al., 2003) integrated force sensors on the handles together with range sensors to support supervised navigation and basic autonomous behaviors. These systems focused mainly on obstacle detection and safe path execution, using user-applied forces as high-level commands. Other early systems, such as PAMM (SPENKO; YU; DUBOWSKY, 2006), incorporated cameras and basic health-monitoring modules. Platforms including JARoW (LEE; OHNUMA; CHONG, 2010; LEE et al., 2011) emphasized user tracking and obstacle avoidance through laser range finders (LRFs) and infrared sensors. Additional developments such as CAIROW (MOU et al., 2012) introduced context-aware assistance using multimodal sensing devices, illustrating how richer sensing

capabilities progressively improved human–walker interaction. Later developments, such as ASBGo++ (ALVES et al., 2017; CAETANO et al., 2016; MARTINS et al., 2014), extended this concept by incorporating gait monitoring and user-position estimation, allowing the walker to adapt its motion according to the user's walking pattern and relative posture.

As sensor fusion techniques and embedded processing became more accessible, more advanced SWs were proposed. The UFES walker (FRIZERA-NETO et al., 2015a; JIMÉNEZ et al., 2018) integrates force sensors, inertial measurement units (IMUs), LRFs, and wheel encoders to support path following, obstacle avoidance, intention detection, and real-time gait monitoring within a shared-control framework. Other systems, such as MOBOT (GERAVAND et al., 2016a; EFTHIMIOU; FOTINEA; GOULAS, 2017; PAPAGEORGIOU et al., 2016), expand interaction capabilities by integrating speech and gesture recognition, body-pose estimation, and adaptive control. More recent platforms, including ISR–AIWALKER (PAULO; PEIXOTO; NUNES, 2017; GARROTE et al., 2018), further explore context-aware assistance using multimodal sensing devices to improve intention detection and navigation guidance according to the user's actions and surroundings. The AGoRA SW (SIERRA et al., 2019) adopts a human-centered design by combining force-based human–robot interaction with adaptive admittance control to assist balance regulation and motion while preserving user autonomy.

More recently, the FriWalk platform (FERRARI et al., 2020) represents a different approach, acting primarily as a navigation aid in which locomotion remains user-driven while the system provides gentle guidance cues to support safe path following and enhance the user's perception of control. Building on this line of work, the UFES vWalker (MACHADO et al., 2023) further extends functionality by combining information from physical and virtual environments. Together, these systems illustrate a clear trend toward richer sensory interfaces and shared-control strategies that balance robotic guidance with user-driven motion. In addition, recent systems have targeted fall-risk reduction by actively stabilizing the user–walker system. For instance, (NADERER et al., 2025) present a robotic assistant walking aid that detects balance disturbances and delivers corrective assistance via controlled actuation. Similarly, (CHALAKI et al., 2025) propose a vision-based fuzzy control scheme to provide more intuitive guidance for stroke survivors with unilateral upper-limb impairments.

In parallel, smart rollators have received increasing attention as an alternative to fully actuated SWs (VERDEZOTO; BALLESTEROS; URDIALES, 2022). These systems extend conventional rollators by incorporating sensing and feedback modules, while keeping propulsion entirely user-driven (SIERRA et al., 2024). Due to their mechanical simpler design, they are easier to deploy not only in clinical or research settings, but also in real-world scenarios, where reliability, cost, and ease of maintenance are critical factors (VERDEZOTO; BALLESTEROS; URDIALES, 2022). Figure 2 presents some smart

Figure 2 – Smart rollators presented in the literature. a) LEA[1]. b) RT.2 [2]. c) Socially assistive walker (SIERRA et al., 2024). d) c-Walker (BALLESTEROS et al., 2016). e) CAMINO [3].

rollators reported in the literature.

Early platforms in this category, such as COOL Aide (HUANG et al., 2005) and i-Walker (CORTÉS et al., 2008; BALLESTEROS et al., 2017), introduced obstacle-based shared control together with 3D environment mapping and vibrotactile feedback. Similarly, the c-Walker (PALOPOLI; ARGYROS; BIRCHBAUER, 2015) integrates radio frequency identification, IMUs, and vision sensors to provide acoustic, mechanical, and haptic feedback for navigation. More recently, the socially assistive SW presented in (SIERRA et al., 2024) combines physical support with simple social and cognitive feedback to assist users during daily living activities. Due to their high practical impact and growing adoption, some commercial platforms have been developed, such as LEA[1], RT.2 [2], and CAMINO [3], which aim to translate research advances into practical assistive solutions.

It is important to highlight, that a common feature shared by SWs is their direct physical interaction with the user, typically through the handles and the supporting frame (MARTINS et al., 2015). This interaction constitutes the primary communication channel between the subject and the device, making its accurate interpretation essential for safe and effective assistance (SIERRA et al., 2024; CIFUENTES et al., 2022a). Besides, the forces

[1] https://www.sparkdesign.nl/projects/lea-care-robot
[2] https://www.rtworks.co.jp/eng/product/rt2.html
[3] https://caminomobility.com/

exchanged provide valuable information about walking intent, balance regulation, and gait dynamics (SIERRA et al., 2021). When monitored over time, these forces can reveal characteristic gait patterns, enabling the identification of changes associated with fatigue, mobility impairments, or progressive motor decline (ELANGOVAN; CHANDRAKUMAR; SAKTHIPRIYA, 2025). Moreover, the dynamic nature of gait-related force information enables the detection of potentially unsafe conditions, such as loss of stability or abnormal loading, which are directly linked to an increased risk of falls (DING et al., 2022). For these reasons, the use of accurate and easy-to-implement sensing solutions plays a central role in the design of SWs (ZOU et al., 2017). The following section discusses the most common approaches used to address this need.

2.3 Sensing of Physical Interaction Forces in SWs

2.3.1 Traditional Force Sensors

Traditionally, a wide range of force-measurement technologies has been used to quantify physical interaction between users and SWs (RESCH et al., 2025; VERDEZOTO; BALLESTEROS; URDIALES, 2022; ZOU et al., 2017; MARTINS et al., 2015). Among these, load cells (LC) based on strain gauges (XU et al., 2015; BALLESTEROS et al., 2016), capacitive sensors (CSs) (ITADERA; CHENG, 2022), force-sensing resistors (FSRs) (LU; HUANG; LEE, 2015; DING et al., 2022), and high-resolution multi-axis force/torque cells (SIERRA et al., 2019; MACHADO et al., 2023; CHALAKI et al., 2025) have been implemented. These sensors have been widely adopted because they provide reliable electrical signals that correlate with applied forces, offer mature manufacturing processes, and well-documented behavior (RESCH et al., 2025). As a result, they have been the standard choice for many platforms where force estimation is required. Figure 3 shows some conventional sensors used in SWs.

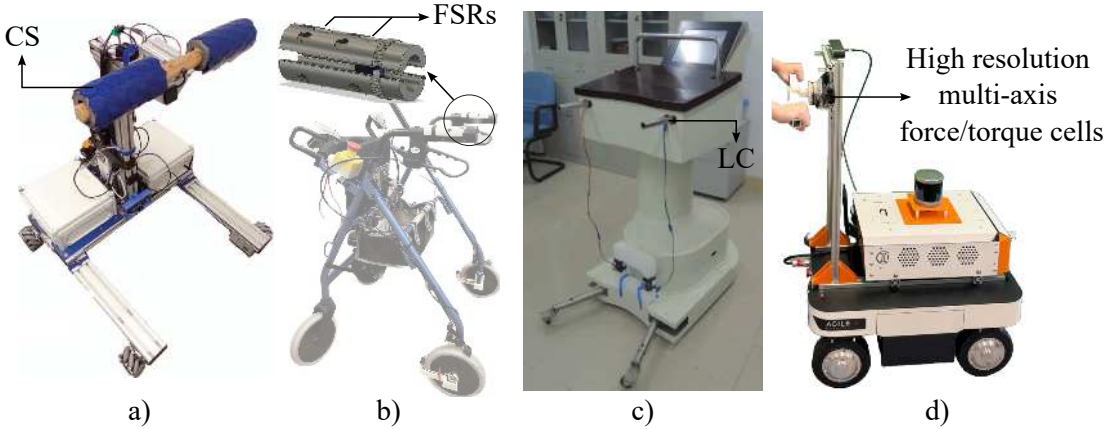

Figure 3 – Traditional sensors implemented in SWs. a) CS (ITADERA; CHENG, 2022). b) FSR (WANG et al., 2024). c) LC (XU et al., 2015). d) (BALLESTEROS et al., 2016). e) High-resolution multi-axis force/torque cell (CHALAKI et al., 2025).

LCs are transducers that convert an applied mechanical load into an electrical signal by measuring the elastic deformation of a metal structure instrumented with strain gauges arranged in a Wheatstone bridge. In (BALLESTEROS et al., 2016), LCs were integrated into the i-Walker handles to estimate spatiotemporal gait parameters by analyzing force differences between the handlebars during walking. Similarly, (XU et al., 2015) employed LCs to measure user-applied interaction forces as inputs to a reinforcement learning-based shared-control strategy, allowing the walker to adapt its assistance level. However, this technology presents some limitations: (1) the output signals are very small and require low-noise amplification, (2) rigid mechanical mounting and careful calibration are required, and (3) measurement accuracy can be affected by wiring length, and sensor misalignment.

FSRs are thin sensors whose electrical resistance decreases when a force is applied (ZOU et al., 2017). They are lightweight, flexible, and easy to integrate into walker handles or support surfaces. In (LU; HUANG; LEE, 2015), FSRs were used to estimate user intent and guide the walker through adaptive motion assistance based on grip forces. Similarly, (HUANG et al., 2021) employed FSRs to detect upper-limb interaction forces during sit-to-stand transfers, enabling intention recognition and compliant control of an assistive walker. In the socially assistive walker presented in (SIERRA et al., 2024), FSRs were integrated into the handles to monitor user interaction forces during daily living activities. Additionally, (DING et al., 2022) used FSRs as part of a multisensor system to detect abnormal force patterns associated with falls. Despite their widespread use, FSRs exhibit lower precision and poorer repeatability compared to load cells. Their output varies significantly between sensors, degrades under sustained pressure or repeated use, and is less stable for long-term measurements or high-force applications.

CSs have also been reported in the literature to capture physical interaction in SWs. These sensors operate by measuring changes in capacitance caused by contact or pressure applied to the sensing surface (ZOU et al., 2017). In (ITADERA; CHENG, 2022), tactile CSs integrated into the walker handlebars were used to detect grasping location and force distribution, enabling the estimation of user interaction forces during single- and dual-hand operation. Although CSs can provide high spatial resolution, their performance strongly depends on the quality of hand–handle contact and requires careful handle design and signal processing (ITADERA; CHENG, 2022). Moreover, the use of distributed CSs increases system complexity in terms of calibration, processing, and control, which can reduce robustness and limit practical deployment outside controlled environments.

Finally, high-resolution LCs and multi-axis force/torque sensors represent one of the most widely adopted technologies for measuring physical interaction forces in SWs (CIFUENTES; MúNERA, 2022). These sensors provide highly precise, stable, and linear measurements, and are capable of detecting small variations in force or torque along one or multiple axes (CIFUENTES et al., 2022a; MARTINS et al., 2015). As a result, they

are well suited for both static and dynamic interaction measurements and offer excellent repeatability. In the current literature, their use has been reported in several platforms to accurately capture user–walker interaction forces for shared control, intention detection, and gait analysis (GERAVAND et al., 2016b; SIERRA et al., 2019; HUANG et al., 2021; CHALVATZAKI et al., 2014; ROHOR et al., 2025). However, their main drawbacks are high cost and increased system complexity. In addition, they require careful mechanical integration, precise calibration, and dedicated signal-conditioning electronics, which can limit their adoption in low-cost or real-world deployments.

In general terms, these sensing solutions have demonstrated broad applicability, but also exhibit important limitations, including mechanical fragility, sensitivity to misalignment, and limited compactness (RESCH et al., 2025; MORENO et al., 2008). Moreover, frequent calibration requirements and high hardware costs increase overall system complexity and reduce scalability (LEAL-JUNIOR et al., 2019a). Collectively, these drawbacks restrict effective integration and can compromise measurement accuracy, reliability, and long-term durability. For these reasons, the development of new sensing technologies that are easy to implement and cost-effective has become an important research challenge and a growing focus in the field (ZOU et al., 2017).

2.3.2 Optical Sensors

OSs have emerged as alternatives for sensing due to their immunity to electromagnetic interference, flexibility, and compactness (LEAL-JUNIOR; NEDOMA; MARTINEK, 2025). Among the different OSs, optical fiber sensors such as polymer optical fibers (POFs) and fiber Bragg gratings (FBGs) have been the most widely adopted (BROADWAY et al., 2019; GARCIA et al., 2025).

POF-based sensors have been employed in a wide range of biomechanical and assistive applications, particularly in scenarios requiring flexibility, compliance, and safe human contact (NGIEJUNGBWEN; HAMDAOUI; CHEN, 2024). Early studies explored their use for monitoring spring deflection in series elastic actuators, enabling indirect torque estimation (CASAS et al., 2019). In the context of gait analysis, POF sensors have been applied to assess plantar pressure distributions and ground reaction forces, providing spatiotemporal information during walking while maintaining portability and user comfort (TAVARES et al., 2021). Furthermore, this sensing solutions have been integrated into wearable and assistive robotic devices, such as exoskeletons, to measure human–robot interaction forces under dynamic conditions (LEAL-JUNIOR et al., 2018).

More recently, this concept has been used to measure user–walker interaction forces. In (REICH et al., 2022), a low-cost POF force sensor was developed and validated against a commercial multi-axis LC, showing comparable performance while reducing system cost and mechanical complexity. To address the viscoelastic behavior of the polymer materials,

the authors used an approximate model with parameters optimized through a genetic algorithm (REICH; FRIZERA; DÍAZ, 2022). However, the proposed sensor includes only a single sensing zone, which limits its use in scenarios with more complex interaction patterns. In addition, the sensor structure was designed for a specific walker, limiting its adaptation to other types of walking frames.

Similarly, FBG-based sensors are recognized for their high-precision measurements in distributed sensing applications (BROADWAY et al., 2019). By inscribing multiple FBGs along a single fiber, these sensors enable distributed or multipoint sensing, which is particularly useful in systems with long structures or multiple contact locations (LEAL-JUNIOR et al., 2019a). In the context of SWs, a study integrated a 5-FBG array into a SW to support multiple functionalities, including structural health monitoring of the walker frame, detection of user movement intention, gait cadence estimation, and detection of floor-induced vibrations for localization and mapping (LEAL-JUNIOR et al., 2019). When compared with commercially available devices, the results showed comparable performance, confirming its suitability for sensing and monitoring in SWs. However, the adoption of FBG technology is restricted by the high cost of interrogation equipment (DIAZ et al., 2019; DÍAZ et al., 2018), underscoring the trade-off between sensing capabilities and accessibility (LEAL-JUNIOR et al., 2019a).

Furthermore, another scalable and cost-effective sensing solution involves the use of optical sensors based on waveguide structures (KONSTANTINOVA; STILLI; ALTHOEFER, 2017; LEVI et al., 2013). This approach relies on overlapping optical signals generated by light emitters and receivers embedded within a compliant waveguide layer (KONSTANTINOVA; STILLI; ALTHOEFER, 2017). When an external force is applied, surface deformations modify the internal light propagation, allowing the sensor to detect contact events and estimate the applied force with high accuracy (LEVI et al., 2013). Compared to POF and FBG-based sensors, this alternative requires fewer wires and the manufacturing process is simpler (LEAL-JUNIOR et al., 2019a; PIACENZA et al., 2020).

This concept has been explored in several robotic and tactile sensing applications. In (KONSTANTINOVA; STILLI; ALTHOEFER, 2017), a fingertip sensor based on overlapping light signals within a deformable waveguide was proposed to detect contact location and normal force, demonstrating its suitability for robotic manipulation tasks. Similarly, (LEVI et al., 2013) introduced a soft optical tactile sensor that exploits changes in light propagation inside an elastomer waveguide to estimate contact forces and pressure distribution over compliant robotic surfaces, enabling distributed contact sensing. Building on this principle, (PIACENZA et al., 2020) presented a sensorized soft structure that combines waveguide-based optical sensing with data-driven models to reconstruct contact forces and deformation patterns more accurately than analytical approaches. Finally, (EL-AZIZI et al., 2024) and (PATEL; CORRELL, 2016) reported integrated waveguide-based

solutions capable of simultaneously estimating contact force and proximity, highlighting the potential of this sensing approach for sensing interaction in robotic systems. Although this technology has great potential, integration into SWs has not been extensively studied in existing literature, representing a clear research opportunity to transfer these capabilities to these mobility assistive platforms.

2.4 Summary and Identified Research Gap

This chapter reviewed the main mobility challenges associated with gait impairments and presented an overview of SWs as assistive solutions that combine mechanical support with sensing and control capabilities. Particular emphasis was placed on the importance of accurately sensing physical interaction forces, as these forces constitute the primary communication channel between the user and the device and provide key information about walking intent, balance, and gait dynamics.

Traditional force-sensing technologies have been widely used in SWs due to their reliability and maturity. However, their deployment is often limited by factors such as mechanical fragility, limited compactness, frequent calibration, and high hardware costs, which hinder scalability and real-world integration. Optical sensing technologies have emerged as promising alternatives, offering advantages such as flexibility, immunity to electromagnetic interference, and high measurement precision. While POF and FBG sensors address some of these limitations, they still face challenges related to simplified designs or costly interrogation units. More recently, waveguide-based OSs combined with data-driven methods have shown strong potential in robotic and tactile sensing, but their application in SWs has not yet been widely investigated.

In this context, a clear research gap can be identified: the lack of compact, cost-effective, and easily integrable sensing solutions capable of accurately estimating user–walker interaction forces while maintaining mechanical simplicity and robustness. To address this need, the main contribution of this work is the validation of an optical force sensor based on a waveguide sensing concept, combined with data-driven machine learning methods for force estimation. The proposed approach aims to deliver a fully integrated sensing solution that relies on affordable fabrication techniques, reduces system complexity, and enhances measurement accuracy, thereby facilitating its practical integration into SWs and supporting their deployment in real-world assistive scenarios.

3 Materials and Methods

This chapter presents the design, fabrication, and validation procedures of the proposed OSs. It describes the selection of electronic and optical components, encapsulation materials, and manufacturing techniques employed during prototype development. Furthermore, it outlines the data acquisition process and the implementation of algorithms for estimating both contact location and the magnitude of the applied force. Finally, it details the validation experiments conducted with the OSs integrated into a SW to evaluate their ability to measure user–device interaction forces during path-following tasks performed by healthy participants.

3.1 First Sensor Version

3.1.1 Design and Manufacturing

The first prototype of the OS was conceived as a compact, low-cost, and easily integrable tactile unit capable of measuring distributed contact forces through light modulation within a deformable medium. The printed circuit board (PCB) was designed with four addressable red-green-blue LEDs (WS2812, World Semiconductor Co., China), four current-limiting resistors of 130 Ω, four decoupling capacitors of 0.1 µF, and five light-sensitive PDs (OSRAM BPW34S, Vishay Semiconductors, United States). The LEDs were selected for their ability to be controlled independently using a single data line, which simplifies the wiring and reduces the need for additional pins in the control unit. Similarly, the PDs were chosen for their large active sensing area of 7 mm², providing a smooth response as light paths are altered (PIACENZA et al., 2020). Figure 4 illustrates the conceptual design of the sensor.

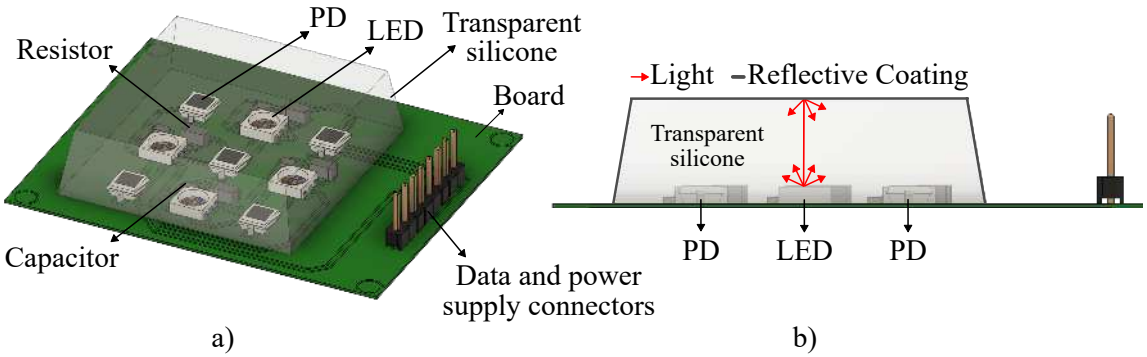

Figure 4 – Proposed sensor. a) Sensor architecture from isometric view. b) Sensor configuration viewed from the front. Besides, the basic concept of the sensor is presented where the emitted light is reflected towards the PDs due to the reflective coating.

The entire system was encapsulated in a transparent layer of silicone (Clear Flex 50, Smooth-On, Inc., United States), which funtioned as a waveguide. This material exhibits a Shore A hardness of 50, providing a balanced combination of flexibility and mechanical resistance to deformation. Additionally, its high transparency makes it highly suitable for light-based applications. The silicone mixture was prepared in a 1:2 ratio, degassed in a vacuum chamber (Resinagem, Brazil) for 10 minutes to eliminate trapped air bubbles that could otherwise scatter light and degrade signal fidelity. Finally, it was left to cure at room temperature for 24 hours. To create the flexible structure with a truncated pyramid shape, a 3D-printed mold made of polylactic acid (PLA) was used to house the uncured resin and the PCB. Once the elastomer solidified, the assembly was demolded and a reflective acrylic coating (Silver 386, Acrilex, Brazil) was applied to the outer surface using a brush (three successive layers at 10-minute intervals) for two reasons: (1) to reflect light back into the transparent elastomer, preventing outward refraction, and (2) to block ambient light, improving signal-to-noise ratio.

The sensing principle of the proposed OS relies on the modulation of light transport within an elastomer when it is mechanically deformed. When the silicone encapsulation is pressed or bent, the surface normal changes, altering the internal reflection and refraction paths of light traveling between the embedded emitters and receivers. These variations in light propagation cause measurable changes in the outputs of the PDs. Because the OS integrates multiple LEDs and PDs, the receptive fields (defined as the regions where deformation alters the PD signal) overlap significantly. As a result, a single contact can stimulate one or more PDs simultaneously. This principle, known as spatially overlapping signals (KONSTANTINOVA; STILLI; ALTHOEFER, 2017), allows the OS to sense contact without requiring isolated or discrete sensing units.

3.1.2 Data Collection and Force Reference Measurements

To convert optical variations into measurable electrical signals, the PD outputs were conditioned using two low-noise operational amplifiers (MCP6024, Microchip Technology Inc., United States), each configured as a transimpedance amplifier. The feedback resistor (R_f) was adjusted to maintain the undisturbed PD signal near the midpoint of the output range, ensuring sufficient headroom under deformation. A 22 pF feedback capacitor (C_f) was placed in parallel to stabilize the circuit by compensating for the capacitance of the PD and the amplifier, thereby preventing oscillations and overshoot, improving the system's stability and temporal response (Microchip Technology Inc., 2017). To minimize impedance loading and reduce noise coupling, additional operational amplifiers (LM258, STMicroelectronics, Switzerland) were configured as voltage followers at the transimpedance outputs. A total of three LM258 chips were used, as each device integrates two operational amplifiers, providing the required number of buffer stages. Data acquisition

was performed using a microcontroller (Teensy 3.6, PJRC, United States) configured with 16-bit analog-to-digital conversion, and signals were sampled at 60 Hz (see Figure 5).

For reference force measurements, a LC (LC201, Omega Engineering, Inc., United States) was mounted on an indenter to record the applied forces (see Figure 6). The indenter was mechanically coupled to a micrometer screw through a custom PLA structure, enabling controlled and repeatable application of normal forces. Using this setup, loads ranging from 0 to 55 N were applied six times to ensure accuracy and repeatability. The OS was positioned on a movable and lockable PLA base, allowing displacement along the X and Y axes for precise alignment with the indenter. This configuration ensured that each PD could be individually aligned and calibrated. This methodological approach made it possible to analyze the interaction and behavior of the sensory components under different loading conditions, which was important to understand the dynamics of the system.

3.1.3 Machine-Learning Algorithms

The signals produced by the sensor were directly correlated with surface deformation, however, building an analytical model to reconstruct the surface state from the collected data could be a difficult task due to the non-linear interaction between the variables, since the signals change in relation to the deformation of the transparent medium, the relative position of the LEDs and PDs as well as the properties of the material, requiring very precise manufacturing (LI et al., 2024). For this reason, the use of purely data-driven based algorithms was an alternative to estimate the parameters of interest from this set of signals (PIACENZA et al., 2020; LI et al., 2024). Specifically, this part of the work was focused on determining the location of a contact and the applied normal force.

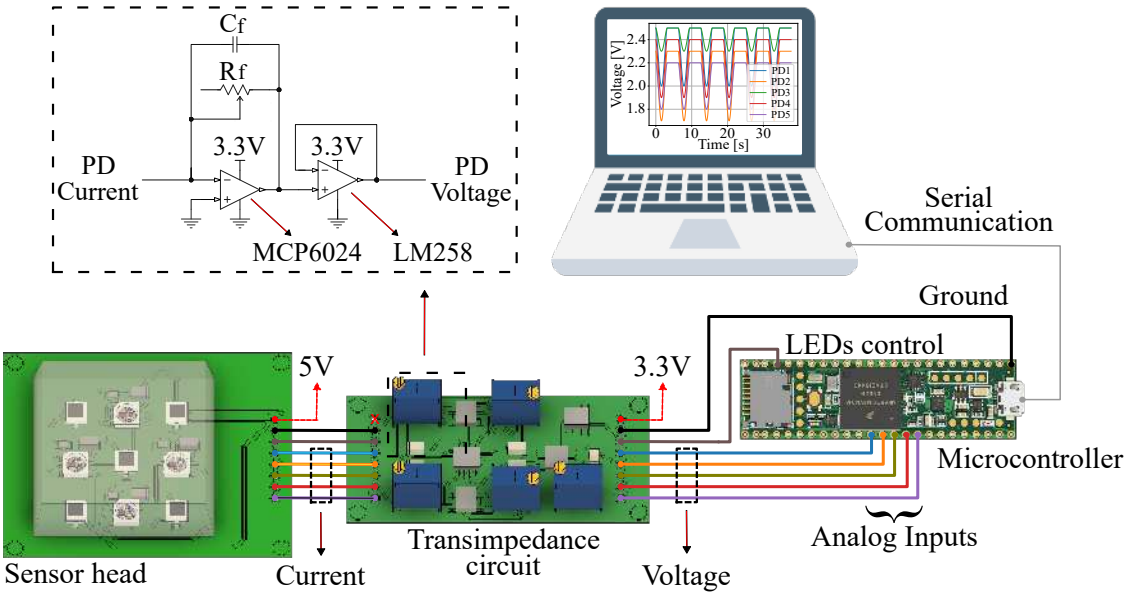

Figure 5 – Complete system configuration.

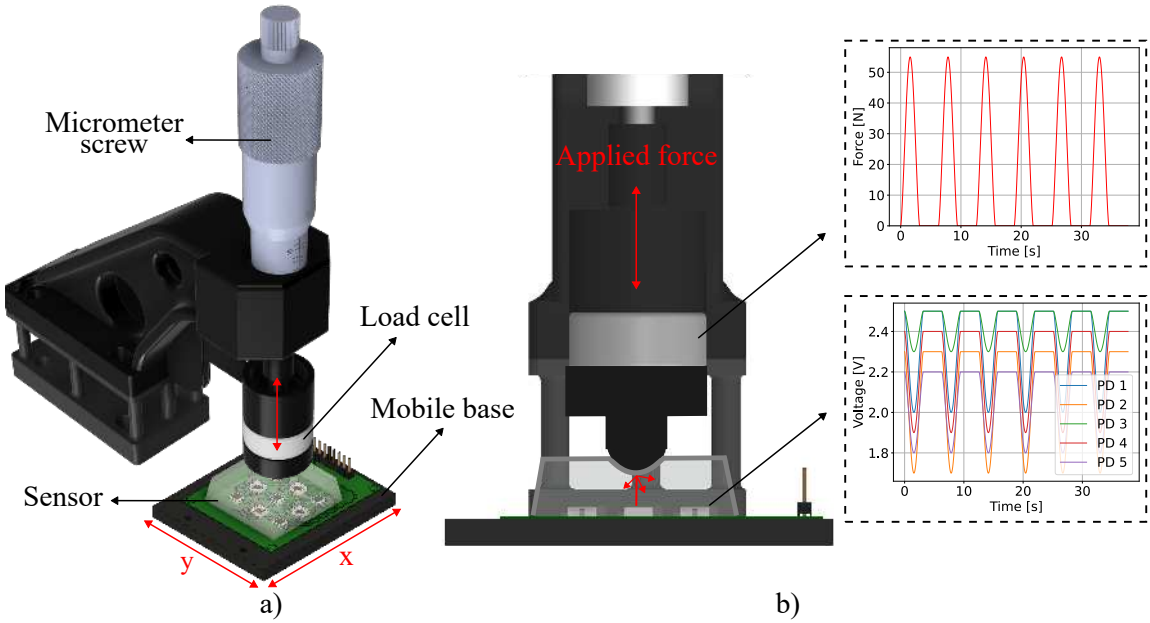

Figure 6 – Mechanical set-up for data collection. a) Proposed structure. b) Sensor surface deformation due the contact with the indenter. The plots show representative examples of the variation in the PD signals and the LC signal.

To address the two prediction tasks considered in this stage, different models were adopted according to the nature of each output variable and following the methodology reported in (LI et al., 2024), where separate models were also used for force estimation and contact-location classification. Since force is a continuous variable, its prediction was formulated as a regression problem and implemented using a feedforward neural network (FNN), which uses five input features (i.e., the data from the PDs). The model was designed with two hidden layers, with 256 units in the first layer and 64 units in the second. The rectified linear unit (ReLU) was used as the activation function, and a Dropout rate of 10% was included to mitigate overfitting. In addition, the Adam optimizer was used with a learning rate of 0.001. The model was trained for 30 epochs with a batch size of 32. The activation function, Dropout technique, optimizer, learning rate, loss function, and performance metric were implemented as described in (PIACENZA et al., 2020), whereas the remaining parameters were experimentally adjusted to achieve the best results. Model performance was evaluated using standard error metrics, including mean squared error (MSE), mean absolute error (MAE), and the coefficient of determination (R^2).

Regarding the prediction of the zone in which the force was applied, a random forest (RF) model was implemented (LI et al., 2024). Zone recognition was formulated as a supervised classification problem, in which each measurement was assigned a categorical label according to the photodiode location that was stimulated during data collection. Specifically, samples recorded while the force was applied over PD1 were labeled as Zone 1; when the force was applied over PD2, samples were labeled as Zone 2, and so on up to Zone 5 (PD5). The RF model was configured with 3 trees, each with a maximum depth of

4 levels. To increase diversity among trees, the split criterion was set to randomly consider the square root of the total number of features at each node. This reduces the risk of trees becoming overly similar and relying on the same dominant features, improving robustness to data variability. Moreover, as regularization measures, each node required at least five samples to allow a split, and each leaf contained at least three samples. The remaining parameters were experimentally tuned to obtain the best results.

It is important to highlight that of the six controlled loads that were applied, the data of the PDs and the LC from the first 5 repetitions were used for training and validating (80% of the data), whereas the last repetition (the remaining 20%) was reserved for testing the model's capability to predict the applied force and the contact zone.

3.2 Second Sensor Version

Previous studies that examined how users interact with walker handlebars (SIERRA et al., 2024; WANG et al., 2024; CHALAKI et al., 2025; ITADERA; CHENG, 2022; LACÔTE et al., 2024) highlight several aspects relevant to the design of sensing interfaces for SWs. First, hand placement along the handle varies considerably during walking, turning, and stabilization tasks, which motivates the need for sensors that cover an extended region rather than a single localized area. Second, stable palm contact across a sufficiently large surface is essential to ensure consistent and reliable interaction during gait. Third, sensing hardware must conform to the curved geometry of commercial handles and allow easy installation and removal to facilitate integration into different walker models and to support regular device maintenance. These findings indicate the need for a sensing interface that accommodates different grip positions, maintains stable contact during movement, and satisfies the mechanical and ergonomic constraints of walking aids.

3.2.1 Design and Fabrication

The second sensor version was designed with an elongated, and linear configuration that follows the curvature of the walker handle, based on previous works (SIERRA et al., 2024; WANG et al., 2024). This geometry increases the active contact surface and improves spatial coverage, enabling the system to capture distributed forces more effectively as users shift their hands or apply uneven loads during gait. Compared with the first prototype, this design prioritizes surface continuity and structural conformity, improving both user comfort and signal reliability during prolonged interaction. The electronic components employed (i.e., LEDs, PDs, current-limiting resistors, and decoupling capacitors) were the same as those described in Section 3.1.1, ensuring hardware consistency between prototypes. The overall architecture of this second OS version is illustrated in Figure 7.

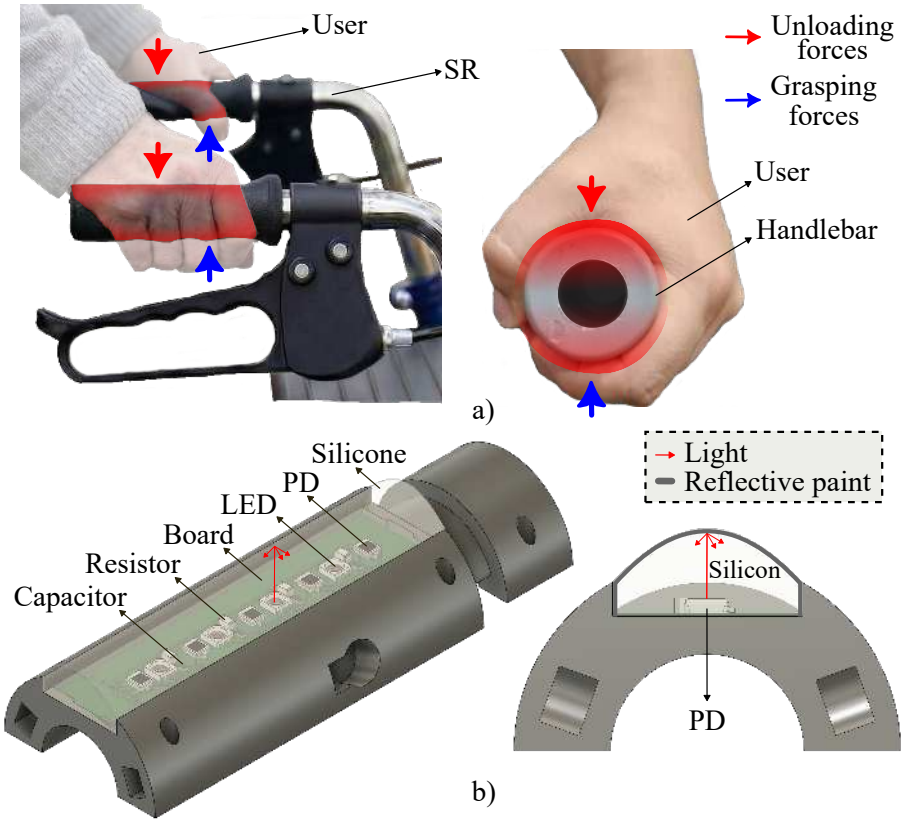

Figure 7 – Handlebar architecture. a) Typical user-handles interactions forces. b) Proposed solution from isometric and front view. Besides, the operating principle is also illustrated, where emitted light is redirected towards the PDs.

3.2.2 Machine-Learning Algorithm for Force Prediction

In this stage, the raw PD signals were preprocessed using a second-order low-pass Butterworth filter with a cut-off frequency of 2 Hz. This step attenuated high-frequency noise while preserving the slow dynamics associated with hand–handle interactions during gait. Regarding force prediction, a FNN architecture was implemented with some modifications relative to the architecture adopted for the first sensor version (see Section 3.1.3), in order to account for the increased spatial coverage, higher number of sensing interactions, and more complex deformation patterns introduced by the second sensor configuration.

For this reason, the refined FNN architecture consisted of three hidden layers with 256, 128, and 64 units, respectively, providing greater representational capacity while maintaining computational efficiency. The model was trained for 90 epochs using a batch size of 32. The calibration dataset was first divided into a training–validation subset (80%) and an independent test subset (20%). To assess the model's stability and generalization capability, a 10-fold cross-validation strategy was applied exclusively to the training–validation subset, which was partitioned into ten equally sized folds. In each iteration, the model was trained on nine folds and validated on the remaining fold, repeating this process until all folds had been used once for validation. The independent

20% hold-out subset was not involved in the cross-validation procedure and was evaluated only once using the final trained model to obtain an unbiased estimate of predictive performance on previously unseen calibration data. As mentioned above, the activation function, optimizer, dropout, and learning rate followed the configuration reported in (PIACENZA et al., 2020), while the remaining parameters were experimentally tuned to achieve optimal results. The regression metrics used for evaluating the model's performance were MSE, MAE, and R^2.

3.2.3 Influence of Encapsulation Material and Illumination Wavelength on OS Performance

The encapsulating material plays a critical role in the performance of OSs, its mechanical compliance and optical transmission properties affect light propagation, deformation behavior, and the resulting PDs outputs. To examine this influence, two silicones with contrasting characteristics were selected: (1) Clear Flex 50 (Smooth-On, Inc., United States), a stiffer and transparent urethane resin already described in Section 3.1.1, and (2) Ecoflex 30 (Smooth-On, Inc., United States), a softer platinum-catalyzed elastomer with higher elasticity and lower transparency. Table 1 summarizes the relevant optical and mechanical characteristics of both materials.

Table 1 – Silicones properties comparison.

Property	**Ecoflex 30**[1]	**Clear Flex 50**[2]
Material	Platinum-catalized	Urethane liquid
Transparency	Translucent	Clear
Mix ratio	1A:1B	1A:2B
Viscosity	3000 cps	250 cps
Tensile strenght	200 psi	250 psi
Pot life	45 minutes	25 minutes
Cure time	4 hours	16 hours
Shore Hardness	00-30	50A
Elongation	900%	500%

Clear Flex 50 was prepared following the same procedure described in Section 3.1.1, including its mixing, degassing, and curing conditions. Ecoflex 30, in contrast, required a separate preparation protocol. The material was mixed at a 1:1 ratio and stirred for three minutes to ensure the activation of the crosslinking components. Then, the mixture was placed in a vacuum chamber (Resinagem, Brazil) for approximately two minutes to remove entrapped air bubbles. Once degassed, the silicone was poured into the 3D-printed mold containing the PCB assembly and cured at room temperature during 4 hours. In both cases, the reflective coating was applied following the same method described in Section 3.1.1. Figure 8 illustrates the appearance of each sensor before and after application

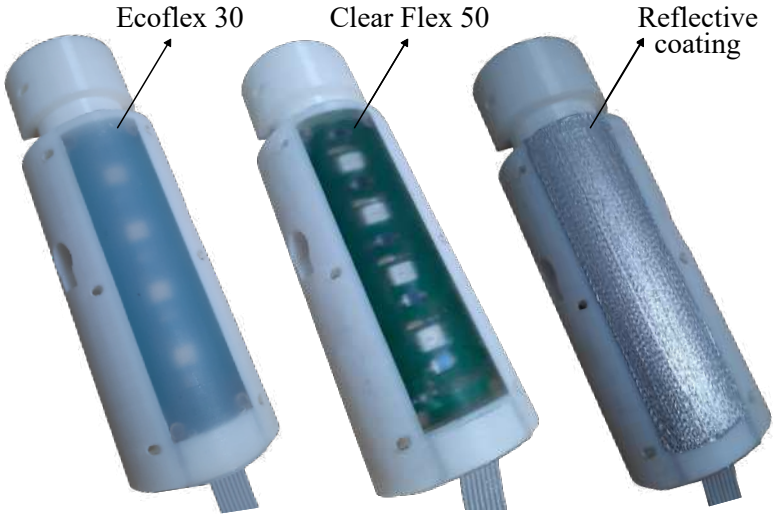

Figure 8 – OS versions fabricated with different encapsulation materials, shown before and after application of the reflective coating.

of the reflective coating.

Each encapsulation material was systematically tested under red ($\lambda = 630$ nm), green ($\lambda = 530$ nm), and blue ($\lambda = 475$ nm) LED illumination to identify the most suitable configuration for accurate estimation. Forces were applied using a five-tip indenter (as described in Section 3.1.2), and data from each configuration were used to train independent FNN models. To validate the generalization capability of the best-performing material–wavelength configuration, an additional test was performed with three load ranges: 10–20 N, 20–30 N, and 30–40 N, respectively. This evaluation provided further insight into the trained model's robustness under different force levels.

3.2.4 Reflective Layer Refinement and Calibration Strategy

After identifying the optimal combination of encapsulation material and LED wavelength, the reflective layer was refined to improve durability. An initial spray coating of instant mirror (Mirror Max, Tog Max, Brazil) was applied three times, with 20-minute intervals between applications and a total drying time of one hour. This was followed by a 1-mm layer of Ecoflex mixed with silver powder (3% of the total silicone mass). This modification preserved the optical properties of the system while enhancing robustness for practical use (see Figure 9). Building on this refinement, four identical OSs were fabricated for the final application (i.e., walking tests with a SW). In particular, the configuration consists of two sensor pairs (one per side), with distinct functional roles:

- **Top sensor:** Dedicated to normal force estimation.
- **Bottom sensor:** Designed to detect finger grasp forces.

[1] https://www.smooth-on.com/products/eco-flex-30/
[2] https://www.smooth-on.com/products/clear-flex-50/

Figure 9 – Ecoflex 30 OS version with the new reflective coating layers.

This symmetrical arrangement enables comprehensive force monitoring during assisted walking while maintaining consistent measurement capabilities on both sides of the walker.

To calibrate the complete system, the experimental setup shown in Figure 6 was employed, following the procedure described in Section 3.1.2. To improve calibration robustness, interchangeable indenters with one to five removable tips were used. The number and arrangement of the tips were changed according to the loading configuration to be tested. For example, when the two-tip indenter was used, different PD pairs were stimulated, including adjacent combinations such as PD1–PD2, PD2–PD3, PD3–PD4, and PD4–PD5, as well as non-adjacent combinations such as PD1–PD3, PD3–PD5, PD2–PD4, and PD1–PD5. Table 2 summarizes the total number of combinations performed per sensor during calibration. This strategy enabled a broader characterization of the sensor response under different loading conditions.

Although all OSs were fabricated using the same design and materials, small variations in emitter–receiver alignment, reflective coating distribution, and/or the viscoelastic nature of the waveguide can introduce nonlinearities in light propagation and deformation response. Thus, training individual networks allowed these variations to be properly captured.

3.2.5 Experimental Validation of Force Estimation

To validate the force estimation capability of the proposed OSs against a commercial reference, an insole-based pressure measurement system (OpenGo Sensor Insoles, Moticon ReGo AG, Germany) was employed. This system provides distributed force measurements,

Table 2 – Summary of all indenter tip configurations used during calibration.

Tips	**Total combiantions**	**Estimulated PDs**
1	5	PD1, PD2, PD3, PD4, PD5
2	8	PD1-PD2, PD2-PD3, PD3-PD4, PD4-PD5 PD1-PD3, PD3-PD5, PD2-PD4 PD1-PD5
3	4	PD1-PD2-PD3, PD2-PD3-PD4, PD3-PD4-PD5 PD1-PD3-PD5
4	3	PD1-PD2-PD3-PD4, PD2-PD3-PD4-PD5 PD1-PD2-PD4-PD5
5	1	PD1-PD2-PD3-PD4-PD5

making it suitable for benchmarking sensing solutions that rely on spatially distributed interaction forces (BRAUN et al., 2015). The system estimates interaction forces based on distributed pressure measurements obtained from 16 capacitive pressure sensors per insole, uniformly distributed across the sensing surface. Each sensing element measures normal pressure in the range of 0–50 N/cm^2, with a resolution of 0.25 N/cm^2 and hysteresis below 1%, enabling reliable capture of localized force contributions. The total applied force is estimated by converting the pressure measured at each sensing element into a local force, based on its effective sensing area, and summing the contributions of all sensors[3].

For the experimental validation, each OS was sequentially positioned on top of the insole, and five controlled loads were applied at different locations across the sensing surface. This setup enabled direct correlation between the distributed force estimates provided by the insole system and the outputs of the OSs. The percentage error (%E), computed as the absolute difference between the reference force measurement and the OS estimate, was used to quantify force estimation accuracy across different load levels.

3.2.6 OSs Performance in Real-World Scenarios

3.2.6.1 Robotic Platform

The socially assistive walker (SAW), a conventional walker frame equipped with multiple sensing modules and feedback components that provide visual, auditory, and user-interface capabilities (SIERRA et al., 2024), was used to validate the performance of the proposed OSs under real locomotion conditions. The four OSs were mounted on the handles to capture user–walker interaction forces (see Figure 10a), while an IMU (BNO080, SparkFun, United States) was positioned below the seat frame to estimate the device's

[3] https://moticon.com/opengo/sensor-insoles

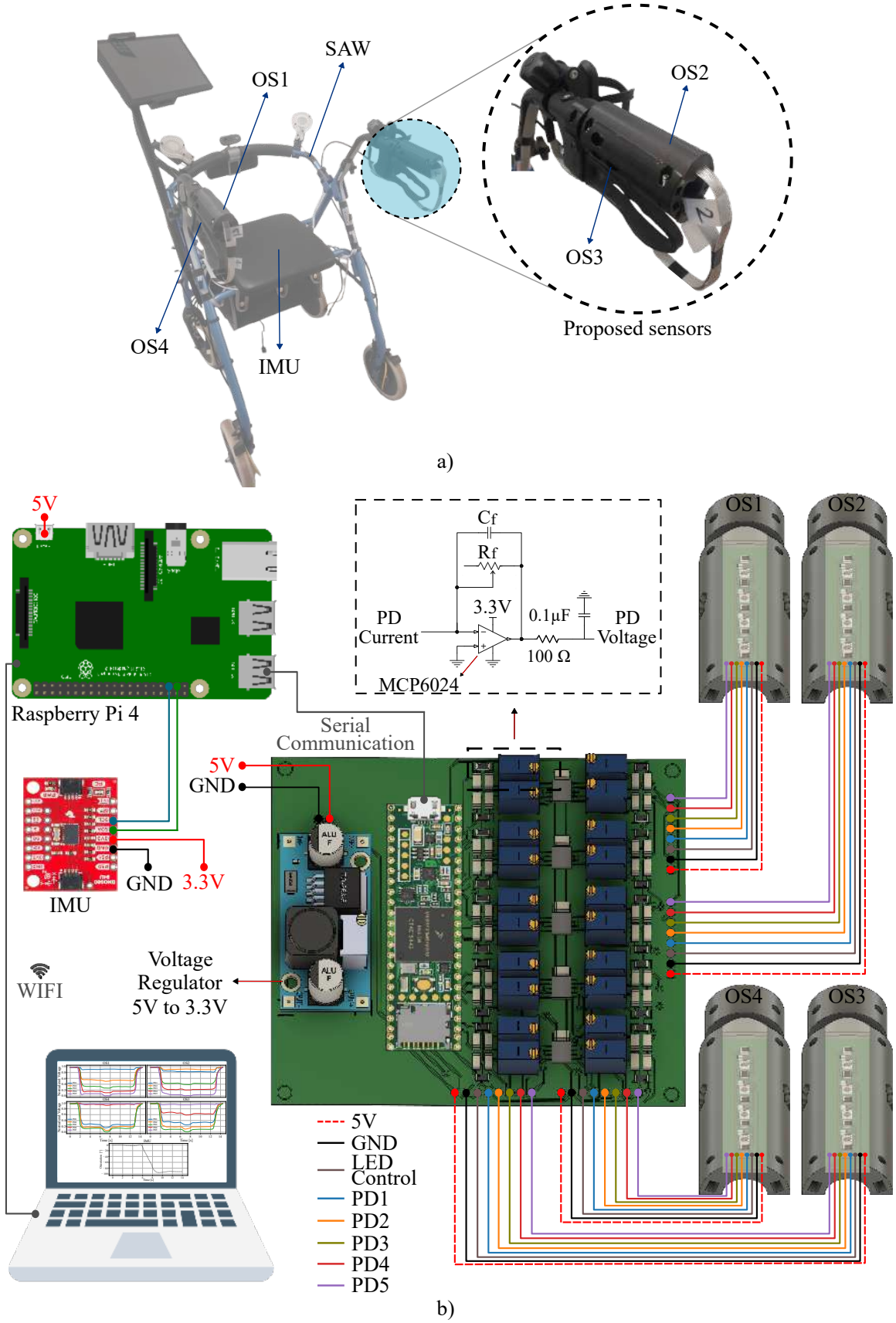

Figure 10 – a) SAW with the proposed OSs mounted on the handles. b) Complete system configuration.

orientation. Additionally, a Raspberry Pi 4 (8 GB RAM; Raspberry Pi Foundation, United Kingdom) running the Robot Operating System (ROS) on a Linux distribution was used to manage data acquisition, communication, and synchronization. An external computer was employed to offload processing from the onboard microcomputer, record experimental data, and serve as the workstation for monitoring the sensor status. The complete system configuration is shown in Figure 10b.

3.2.6.2 Participant Recruitment

Ten healthy volunteers participated in the study (six males, four females; age: 26.10 ± 5.15 years; height: 1.73 ± 0.12 m; weight: 68.40 ± 10.71 kg). Table 3 details the demographic data of the participants. The inclusion criterion was the absence of gait-affecting pathologies, and participants with physical or cognitive conditions were excluded. Although the sample size was limited, it is consistent with previous studies validating sensing systems on walker handlebars (WANG et al., 2024) and interaction strategies based on handle-mounted systems (CHALAKI et al., 2025).

Table 3 – Demographic information of the volunteers involved in the study.

Subject	**Gender**	**Age [y.o.]**	**Height [m]**	**Weight [kg]**
1	F	25	1.65	60
2	F	25	1.60	55
3	F	23	1.60	62
4	F	22	1.63	57
5	M	23	1.77	70
6	M	37	1.83	90
7	M	25	1.79	70
8	M	32	1.72	70
9	M	29	1.80	80
10	M	20	1.64	70

3.2.6.3 Ethics Statement

The experimental protocol was approved by the University Research Ethics Committee. All participants were informed of the study's scope and data storage procedures and were free to withdraw or decline the use of their data at any time.

3.2.6.4 Experimental Procedure

All trials were conducted in the Assisted Living Studio of the Bristol Robotics Laboratory, a controlled indoor environment designed for evaluating assistive technologies. The experimental area provided consistent ambient lighting and marked floor cues to guide the prescribed trajectories. No obstacles or external distractors were present, ensuring

that variations in the OSs' outputs were attributable to user interaction rather than environmental disturbances.

The walking tasks were defined as follows:

- **Straight (ST)**: participants traversed a 3 m straight path.
- **Left turn (LT)**: participants walked 2 m, executed a 90° left turn, and continued for another 2 m.
- **Right turn (RT)**: identical to the left-turn task but turning 90° to the right.

Each task was performed three times at a self-selected, comfortable walking speed, with short rest periods provided between trials. Participants were allowed to hold the handles naturally, without constraints on grip strategy or force application. A practice trial was completed prior to data collection to familiarize participants with the setup.

3.2.6.5 Data Analysis

To analyze the data obtained during the path-following experiments, two descriptive features were extracted from the force signals estimated by each OS: (1) the mean value computed over the duration of each trial, and (2) the peak value observed during the same interval. These features were selected to capture both the overall interaction level and the maximum force exerted by the participant during the task. First, the extracted features were averaged across the three repetitions for each sensor, yielding a single representative value per participant and task. Subsequently, the results were aggregated across all participants by computing the mean and standard deviation over the ten subjects. All reported values are presented as mean ± standard deviation, providing a quantitative summary of inter-subject variability.

Regarding the statistical analysis, data normality was assessed using the Shapiro–Wilk test. The repeated-measures ANOVA test was applied to normally distributed data, whereas the Friedman test was used for non-normally distributed data. When significant differences between trajectories were detected, post-hoc pairwise comparisons were performed using Bonferroni test for parametric data and Wilcoxon test with Bonferroni correction for non-parametric data. All statistical analyses were performed in RStudio, with the significance level set at 5% ($p - value < 0.05$).

4 Results and Discussion

This chapter presents the experimental evaluation of the two prototype versions of the proposed OSs. First, the signal behavior, force estimation, and contact-location capabilities of the initial version are analyzed, including the results obtained using FNN architectures for force prediction and an RF classifier for contact localization. Subsequently, it reports the assessment of the second version through a series of material–wavelength comparisons, multi-point indentation tests, and validation using a commercial reference system. Finally, the chapter describes the integration of the OSs into a socially assistive walker and the protocol used to evaluate their ability to capture user–device interaction forces during path-following tasks performed by real subjects.

4.1 First Sensor Version

4.1.1 Sensor Response during Indentation Tests

Figure 11 presents the results obtained when force was applied directly to PD1. As mentioned previously, six repetitions were performed under identical loading conditions, and the response of each PD was recorded. The signals shown correspond to the typical behavior observed during a single-point indentation and illustrate how the stimulated PD and its neighboring sensing elements are effected, indicating how deformation propagates across the surface.

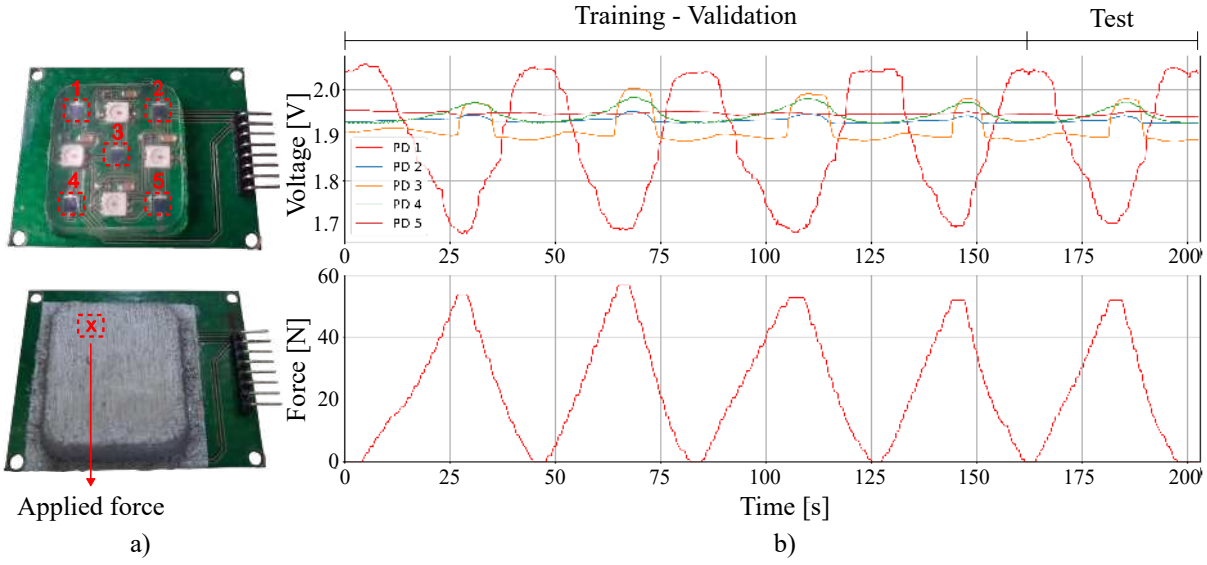

Figure 11 – Results obtained from the sensor response. a) Sensor configuration showing the location of the PDs and the position where the force was applied. b) Signal contribution of each PD and the reference force measured by the LC.

As can be seen, the PD that was directly stimulated showed a response proportional to the increase in the applied force, confirming its sensitivity in the contact region. The neighboring PDs also exhibited variations in response, although with smaller magnitudes. This behavior reflects how deformation propagates across the surface, indicating that the system can provide information not only at the point of contact but also about how the load spreads through the encapsulation material. This transverse sensing capability suggests that the sensor can operate as a deformable, and fully measurable surface, which may be advantageous in applications where continuous and distributed loads must be monitored, enabling the assessment of more complex and spatially extended pressure patterns.

4.1.2 Performance of the Learning Algorithms

After conducting the same single-point indentation procedure on all five PDs, the full dataset was used to train an FNN for force estimation and a RF model for contact-location classification. The performance metrics for both models are summarized in Figure 12. As shown in Figure 12a, the FNN achieved an R^2 of 0.98, with an MSE of 5.87 and an MAE of 1.79, indicating its ability to capture the relationship between the PD signals and the applied normal force with high accuracy. Similarly, Figure 12b presents the confusion matrix for the RF classifier, which reached an accuracy of 0.98 and correctly identified the majority of contact locations. These results indicate that both architectures performed effectively within their respective estimation and classification tasks.

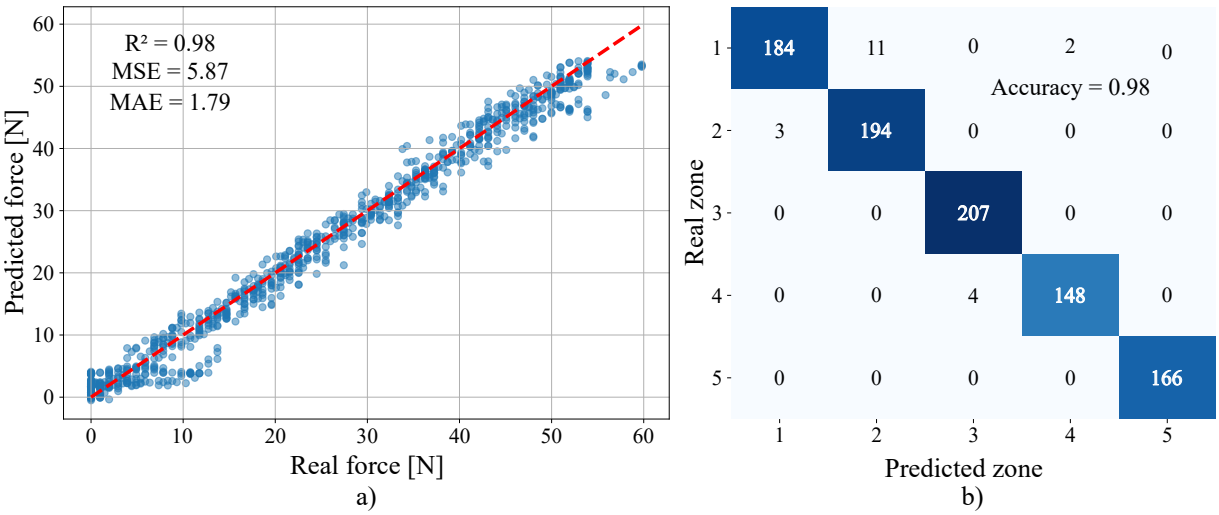

Figure 12 – Performance metrics obtained after training. a) Results of the FNN for force estimation. b) Results of the RF model for contact-location classification.

Figure 13 presents the results obtained from the trained models predicting both the contact zone and the applied force. As shown, the FNN outputs exhibit strong agreement with the reference values. Specifically, an average error of 2.42% was obtained, with the

highest error observed for PD3 at 2.61%. This behavior is consistent with the findings in (PIACENZA et al., 2020), where higher errors (up to 5%) were observed when working with loads between 9 and 16 N. This increase could be related to the magnitude of the applied load, since the error is mainly observed in the range from 30 to 55 N. However, when compared to the applied forces in (PIACENZA et al., 2020), the error is still relatively low. Moreover, as PD3 is positioned at the center of the array, it may be more sensitive to deformation propagation, which could induce more complex patterns for the FNN.

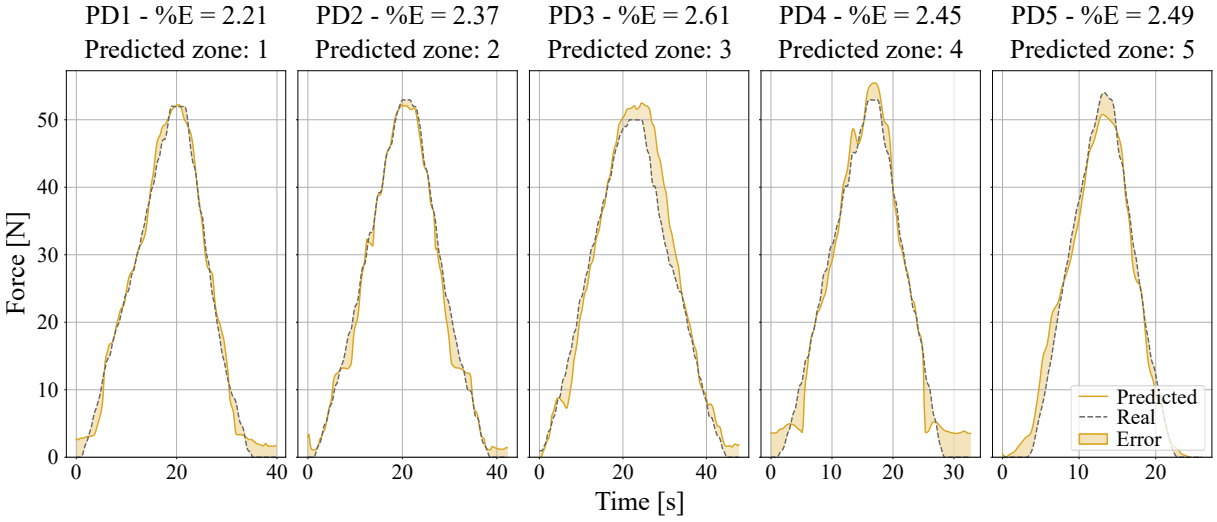

Figure 13 – Results obtained from the proposed models. The yellow line shows the force estimated by the FNN, the gray dashed line represents the reference force, and the yellow shaded area indicates the error. The predicted contact zone shown corresponds to the output of the RF classifier.

As for PD4, the results show a reduced ability to predict forces below 4 N. As reported in (PIACENZA et al., 2020), this behavior is expected, since errors of up to 10% were observed when working with low-magnitude loads. This suggests that reducing the effective measurement range of the sensor for small forces could be beneficial for maintaining accuracy in this region. According to the literature, users typically apply forces greater than 5 N during path-following tasks (JIMENEZ et al., 2024; CIFUENTES et al., 2022b), indicating that this adjustment would not compromise practical usability. Additionally, because the sensor operates as a fully deformable surface, compensation strategies could be implemented to mitigate this limitation if required.

Regarding the classification of the force application zones, the RF model demonstrated high performance. With an accuracy of 0.98 after training, it was able to correctly predict the five zones where loads were applied. This high performance highlights the model's inherent ability to handle complex data and establish clear patterns in multi-categorical classification problems. Furthermore, this result is supported by what is reported in (LI et al., 2024), where the effectiveness of RF in this type of tasks is emphasized, highlighting its robustness to variations in the data and its ability to generalize correctly.

4.2 Second Version

4.2.1 Color and Silicone Response Evaluation

Figure 14 shows the results obtained when pressure was applied to the OSs, comparing the response of the two encapsulation materials under red illumination. In both cases, the PD signals decrease as the applied force increases, confirming that the OSs can translate mechanical deformation into electrical signals. The curves also reveal consistent behavior across repetitions, indicating stable light–material interaction and reproducible deformation patterns.

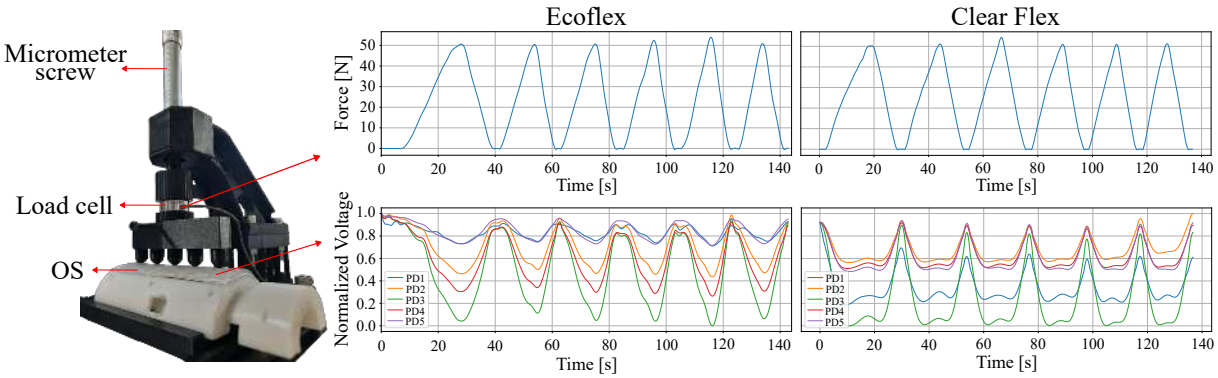

Figure 14 – Comparison of the OS response for both encapsulation materials. The right panel shows the experimental setup, and the left panel presents the normalized PD outputs and the reference force measured by the LC.

For EcoFlex, the results indicate that the OS response decreases with the applied force, demonstrating its ability to translate mechanical deformations into electrical signals. Among the individual PDs, PD3 shows the highest sensitivity, likely due to its central position within the OS, making it more responsive to pressure changes and material deformation. This location allows PD3 to directly capture induced deformations, enhancing light transfer to its active surface and optimizing its response. The geometrical distribution of the PDs ensures uniform coverage and optimal sensitivity across the entire sensor area. Additionally, the OS fabricated with ClearFlex saturates faster, likely due to its transparent resin. In contrast, EcoFlex reduces this effect because its cloudy color and texture increase signal dispersion, introducing controlled signal dispersion. Although EcoFlex has higher losses, its flexibility prevents saturation and improves its response to pressure changes. These findings align with previous studies demonstrating that silicone properties influence light transmission (XIE et al., 2025; LIN et al., 2010).

Table 4 presents the metrics obtained by the FNNs across the different material–wavelength combinations. The results demonstrate that the Ecoflex outperforms Clear Flex, achieving the lowest MSE (Validation: 4.72 ± 0.31 - Test: 4.96), MAE (Validation: 1.61 ± 0.04 - Test: 1.79), and a high R^2 (Validation: 0.98 ± 0.01 - Test: 0.97) with red light, indicating accurate FNN predictions. While all configurations show strong R^2 values

(≥ 0.94), Clear Flex performs worse, especially with blue light, which exhibited the highest prediction errors. Ecoflex's superior performance may be attributed to its opto-mechanical properties, enhancing light transmission under deformation. Additionally, the results obtained with red light may be associated with the spectral sensitivity of PDs, which is higher in the near-infrared region (approximately 900 nm). Consistent with (FRANK et al., 2022), red color also enhanced sensor response, reinforcing that material–wavelength interactions affect sensitivity (XIE et al., 2025).

Table 4 – Performance metrics of the FNN under different material–wavelength configurations obtained during the validation stage. The data highlighted in bold indicate the best results.

Silicone	Color	MSE	MAE	R^2
Ecoflex	**Red**	**4.72 ± 0.31**	**1.61 ± 0.04**	**0.98 ± 0.01**
	Green	6.10 ± 0.24	1.88 ± 0.11	0.97 ± 0.01
	Blue	11.08 ± 0.56	2.35 ± 0.37	0.96 ± 0.02
Clear Flex	Red	5.85 ± 0.43	1.95 ± 0.09	0.97 ± 0.01
	Green	7.91 ± 0.26	1.91 ± 0.04	0.96 ± 0.02
	Blue	15.03 ± 0.60	3.55 ± 0.06	0.94 ± 0.02

Finally, Figure 15 shows the response of the trained model for the best-performing configuration (i.e., Ecoflex and red color) under a new force test. The comparison between the estimated (i.e., OS data) and reference values (i.e., LC data) shows that the FNN was able to reproduce the applied loads consistently. The model achieved an average error of 5.56 %. For comparison, (PIACENZA et al., 2020) reports that estimation errors can increase by up to 5% when the sensor operates under higher load ranges. While the proposed model exhibits a higher error, it is important to note that it was validated across a broader range of loads, spanning from 0 to 40 N. Besides, errors below 10% have been reported for force-sensing applications in SWs (BALLESTEROS et al., 2016), supporting the suitability of the proposed approach.

4.2.2 Calibration and Force Estimation Validation

Figure 16 illustrates the heatmap of the OS1 response under different indentation conditions, ranging from one to five contact tips. It is important to highlight that, the illustration provides a qualitative spatial representation of how the OS response is distributed over the sensing surface. To generate these maps, a representative instant was selected from each test at the point of maximum applied force. The PD signals at that instant were then baseline-corrected and normalized to make their relative magnitudes comparable. These normalized values were assigned to the known physical positions of the PD within the OS, and a continuous 2D field was constructed by representing each response as a Gaussian distribution centered at its corresponding location. The final heatmap was obtained by superimposing these Gaussian contributions over a regular

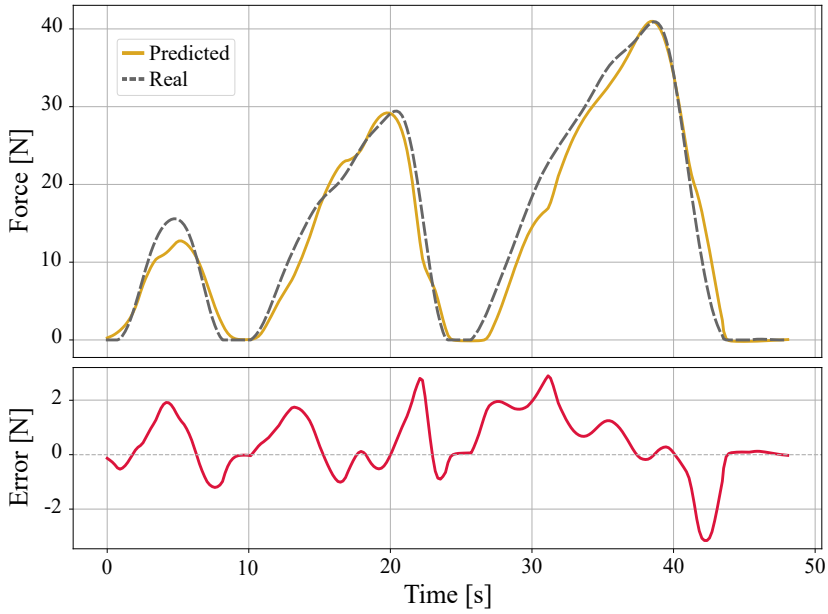

Figure 15 – Results obtained from the trained model with the data of the OS fabricated with Ecoflex and using red light.

grid and normalizing the resulting field between 0 and 1. Therefore, the map should be interpreted as a smooth interpolation of the relative OS response across the surface.

In this sense, the single-point indentation produces a localized peak at PD1, which is directly aligned with the stimulated position. This confirms the sensor's ability to resolve single-point indentations and establishes a reference for precise localization under simple loading scenarios. Nevertheless, a slight activation is also observed in PD2, suggesting continuity across the surface due to signal overlap, reflecting the light propagation within the silicone (KONSTANTINOVA; STILLI; ALTHOEFER, 2017; PIACENZA et al., 2020).

In the second case, two activation lobes appear over PD4 and PD5, indicating simultaneous contact points. The partial overlap between adjacent PD responses preserves surface continuity and enables reliable detection of multi-point loads. While the overall distribution remains balanced, PD5 exhibits slightly higher intensity than PD4, suggesting sensitivity variations potentially caused by localized differences in silicone curing, non-uniformities in the reflective layer, or fabrication-induced variations (MENEGARDO; LEAL-JUNIOR, 2025). The three-tip configuration generates a more distributed response, with PD1, PD3, and PD5 showing the strongest activations. Despite the added complexity, the three peaks remain clearly distinguishable, confirming the sensor's ability to resolve multiple contact points. Moreover, the overlapping regions between activations enhance spatial coverage and contribute to improved measurement stability.

The four-point case shows strong responses at PD1, PD2, PD4, and PD5, with a slight increase in overlap in the central region. Furthermore, the peaks remain distinguishable, indicating that the sensor maintains adequate separation despite the added

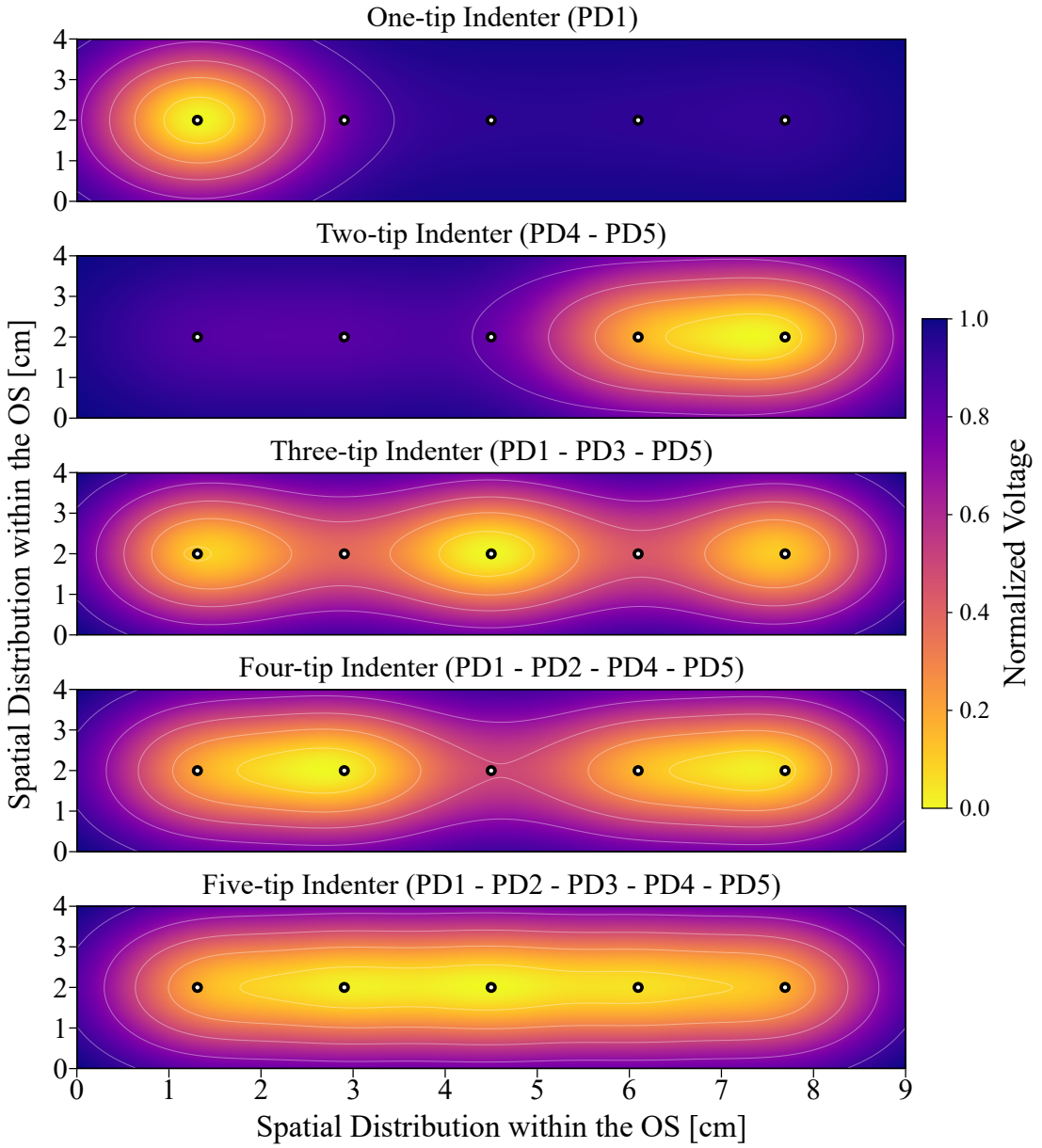

Figure 16 – Response of the OS under one- to five-tip indentations. The black circular markers indicate the PD locations. Warmer tones (yellow) denote higher signal levels and cooler tones (purple) represent lower responses.

complexity of the load. Finally, the five-point indentation results in a smooth and continuous distribution across the sensor surface, with all PDs showing high and relatively uniform responses. This result confirms that the sensor can handle distributed loads without saturating or losing resolution, validating its sensing capability across the entire range. These results demonstrate that the calibration strategy successfully captures both localized and distributed force inputs, ensuring spatial encoding across all tested configurations.

After completing the tests (21 combinations per OS), individual FNNs were trained for each sensor using their respective calibration datasets. The results revealed consistent performance across the four OSs. Among them, OS4 achieved the best performance, showing the lowest MSE (Validation: 3.11 $\pm$ 0.55 - Test: 3.33) and MAE (Validation: 1.18

± 0.10 - Test: 1.24) and the highest R^2 (Validation: 0.98 ± 0.02 - Test: 0.98). In contrast, OS2 exhibited the lowest performance, with an MSE of 6.08 ± 0.42 (Test: 6.27), an MAE of 1.73 ± 0.03 (Test: 2.15), and an R^2 of 0.97 ± 0.03 (Test: 0.96), likely reflecting variations in PD alignment, light propagation, or material deformation during fabrication. Figure 17 summarizes the metrics obtained for all four sensors.

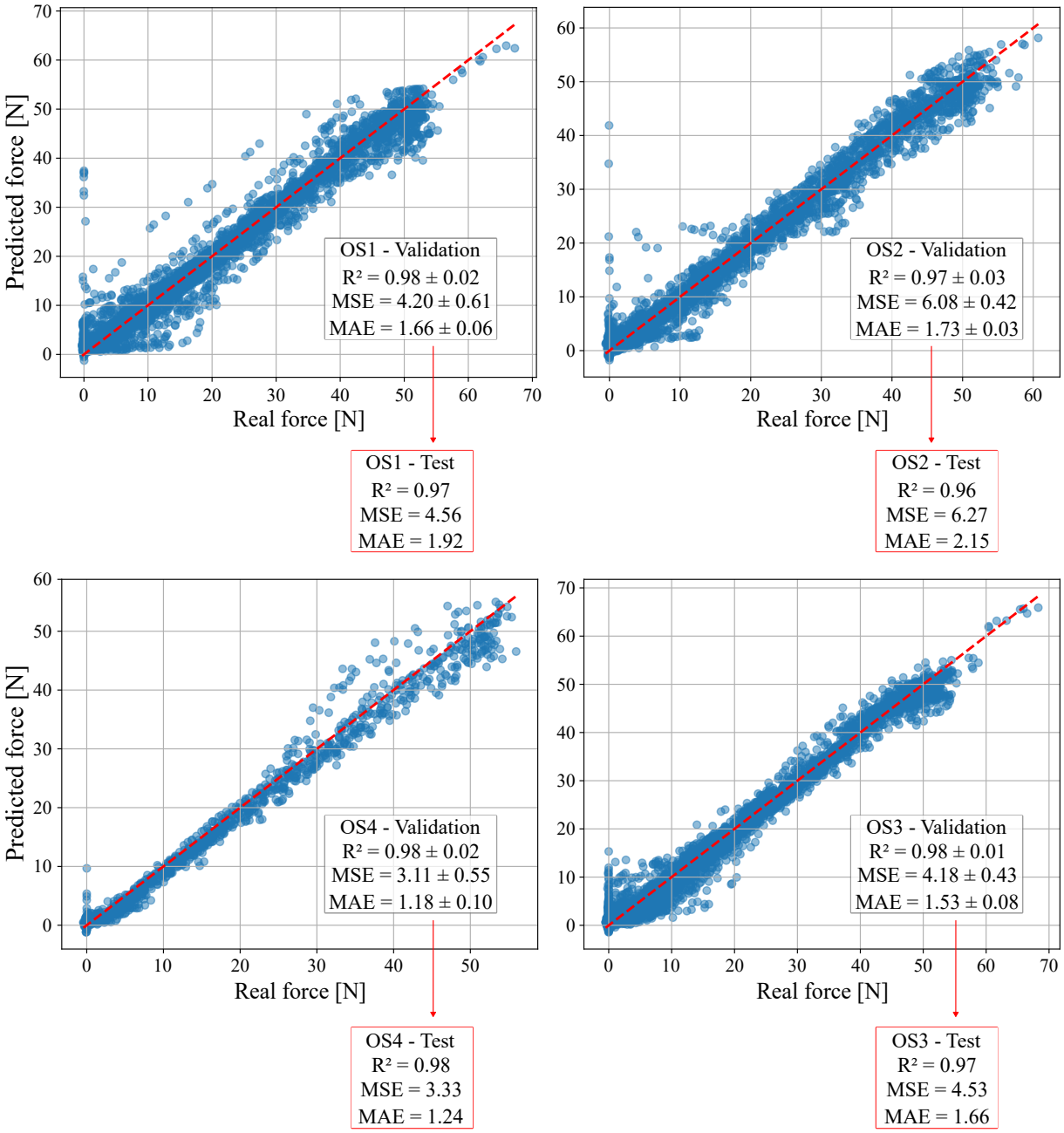

Figure 17 – Performance metrics of all OSs obtained with the calibration data during the validation stage. The metrics presented on the red box were obtained during the test stage.

Figure 18 presents the static validation test of OS1 using a commercial system as the reference. As illustrated in Figure 18a, the sensor was placed on top of the insole and subjected to five controlled loading conditions. Figure 18b shows the PD responses

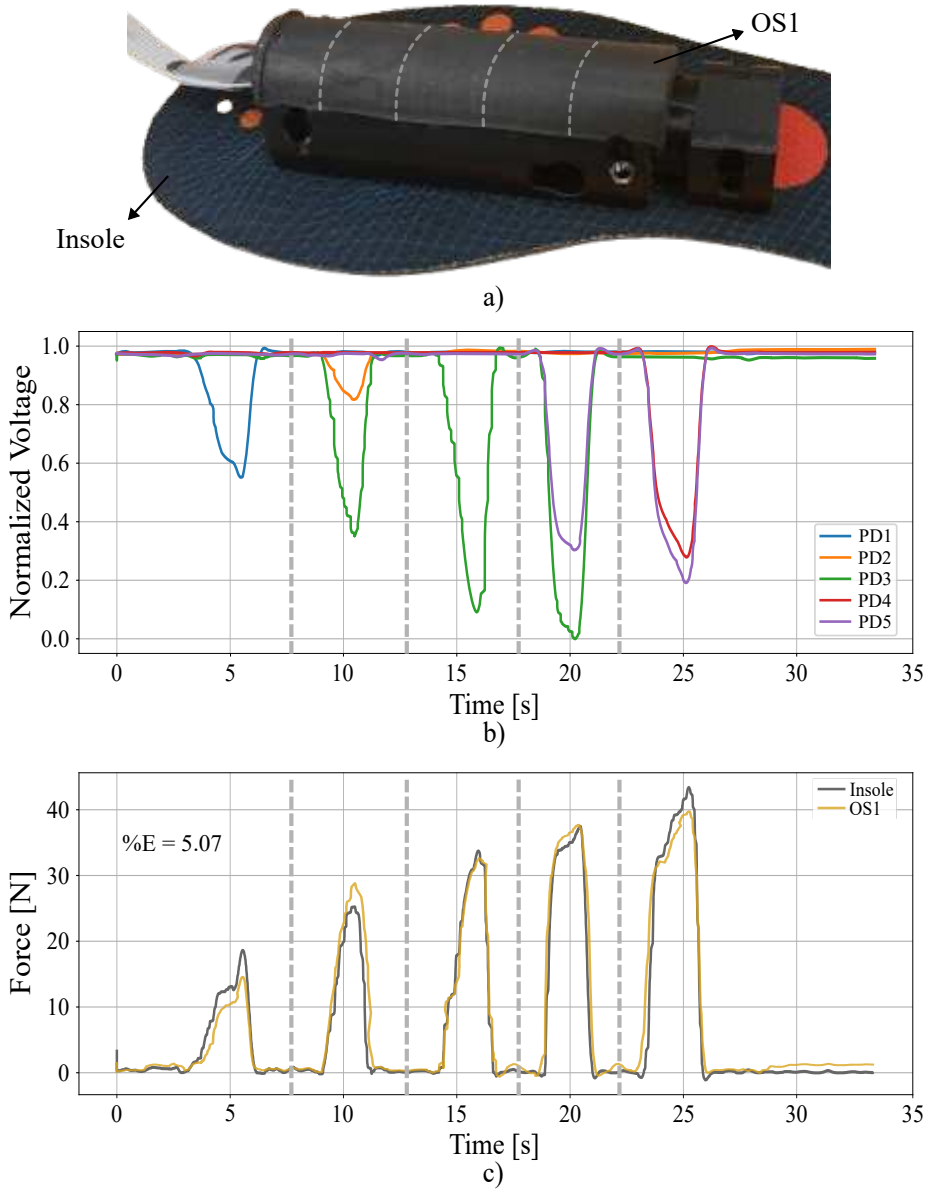

Figure 18 – Experimental comparison between OS1 and the commercial reference system. a) Experimental setup. b) Raw PDs signals. c) Comparison between the force estimated by OS1 and the reference force measured by the insole.

during successive force applications, where a sequential activation pattern is observed. Among the PDs, PD3 exhibits the largest variation, consistent with its central location and higher sensitivity, while the remaining PDs also display distinguishable responses. The partial activation of neighboring PDs highlights the continuity within the waveguide. Figure 18c compares the force estimated by OS1, using its trained FNN, with the reference force obtained from the insole. The results demonstrate strong temporal alignment and amplitude agreement across trials, yielding an average estimation error of 5.07%. This outcome is aligned with recent reports on encapsulated sensors (PIACENZA et al., 2020) and achieves lower error rates compared to quasi-distributed POF-based systems with coupled PDs, which have reported errors arround 5.40% (MENEGARDO; LEAL-JUNIOR,

2025).

Notably, the OSs located on the bottom also exhibited low estimation errors, with OS3 achieving 4.97 % and OS4 delivering the best performance at 4.37 %. In contrast, OS2 showed a slight increase to 5.78 %. This minor deviation is consistent with the calibration accuracy previously observed, likely caused by small variations introduced during the manufacturing stage. These results reflect the same trends identified during calibration, where OS2 exhibited reduced performance and OS4 demonstrated superior accuracy. The alignment between offline metrics and the errors measured during validation indicates that the predictive performance of the FNN is preserved when transitioning from controlled calibration tasks to experimental conditions. This consistency suggests that the proposed framework captures the intrinsic differences introduced by manufacturing and material properties and reliably translates them into predictable performance.

4.2.3 Experimental Validation During Walking Trials

The OSs were integrated into the SAW and evaluated during three path-following tasks. A total of 90 walking trials were conducted, including straight and turning maneuvers. Figure 19 presents the results from the RT test, highlighting the individual contributions of the PDs of each OS.

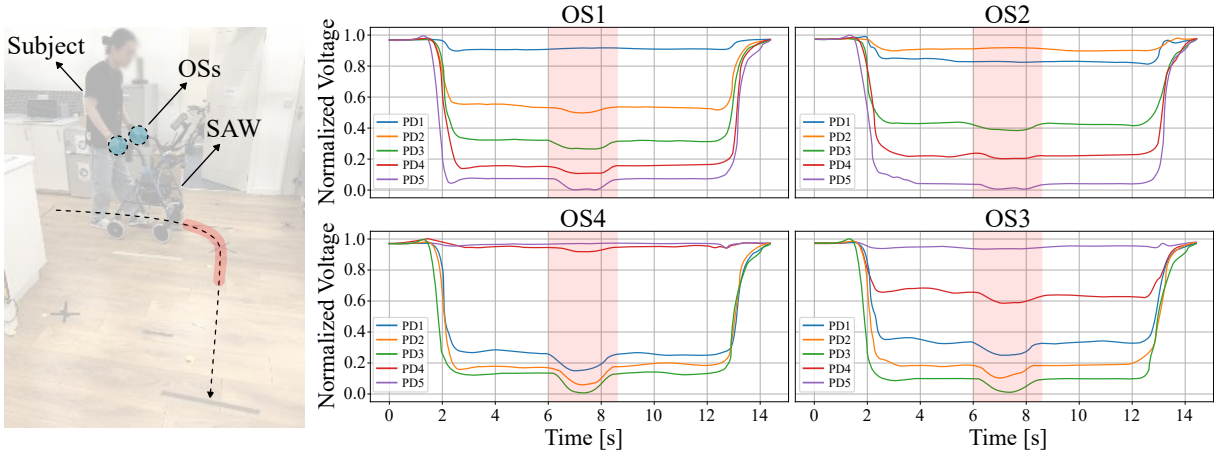

Figure 19 – Results obtained during the RT test of one subject. The red shadow highlights the turning area.

The signals recorded by each PD reflect the force applied by the user on the SAW handlebar, providing information on grip patterns and force distribution. Distinct activation profiles are observed, confirming that the geometric arrangement of the PDs allows for the detection of spatial variations. Specifically, the OSs located at the top (i.e., OS1 and OS2) show activation patterns indicating that the force was directed mainly toward their front regions, while the lower sensors reveal a distribution toward the rear. This distinction suggests that the proposed configuration allows the distribution of applied forces to be captured. Besides, during the turn section (represented in the shaded area), a

change in PD activation can be observed. In particular, OS1 and OS4 exhibit an increase in signals, indicating greater force on that side of the handlebar. This behavior suggests that the user redistributes the force to the outer side to compensate for the turning maneuver, which is consistent with the expected in assisted locomotion tasks (SIERRA et al., 2021).

On the other hand, Figure 20 shows the forces estimated by the OSs during the

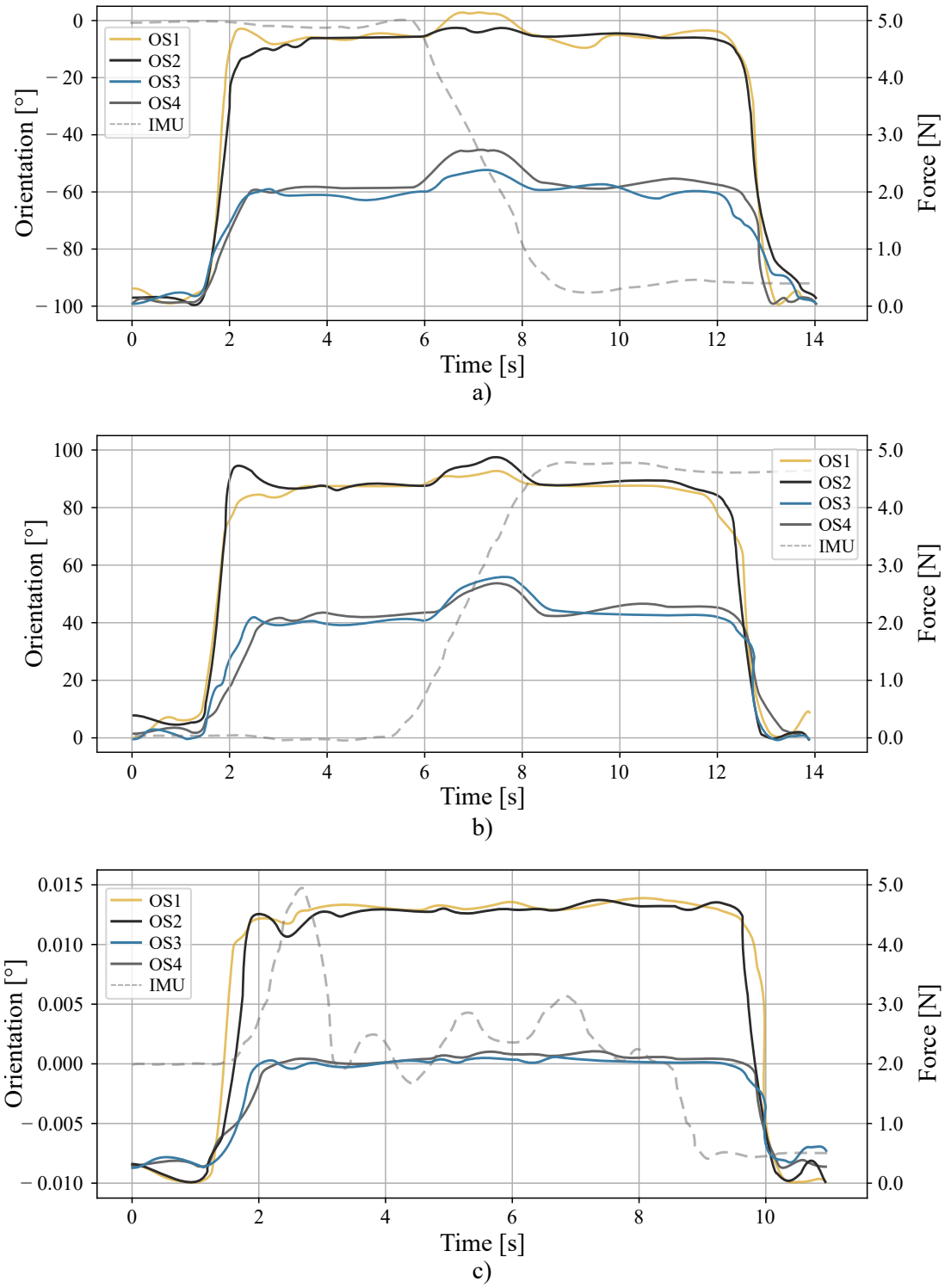

Figure 20 – Force estimation results from the OSs across the three path-following tasks. a) RT. b) LT. c) ST.

walking tasks, with the IMU orientation used to identify the task stages. During the RT maneuver (Figure 20a), OS1 and OS4 recorded higher magnitudes than their opposite counterparts, OS2 and OS3 respectively, reflecting increased loading on that side of the walker. Conversely, during the LT (see Figure 20b), OS2 and OS3 exhibited higher values, confirming the reliable detection of directional force redistribution. This behavior is consistent with the findings reported in (LEAL-JUNIOR et al., 2019), where FBG sensors located on the outer side of the turn exhibited larger wavelength shifts, indicating greater loading on that side of the walker during maneuvers. Additionally, Figure 20c shows the results obtained during the ST task. Unlike the turning maneuvers, the force distribution across the four OSs remains more balanced, with no clear dominance of one side over the other. The upper sensors continue to exhibit higher amplitudes than the lower ones, reflecting the user's unloading force on the handlebar, while the lower sensors capture smaller gripping forces. This stability in the signals indicates that the sensors respond consistently under steady locomotion, providing a reliable baseline to contrast against the variations observed during directional changes.

Finally, Figure 21 summarizes the average peak force values estimated by the four OSs across the three walking tasks, with error bars representing inter-participant variability. A clear distinction emerges among the OSs, indicating that the proposed system reliably captures differences in user-walker interaction under diverse locomotion conditions. During turning maneuvers, the sensors located on the outer side of the turn exhibit the highest magnitudes. Specifically, OS1 and OS4 record greater values during RT, while OS2 and OS3 dominate during LT. This pattern is consistent with the temporal profiles previously shown in Figure 20a–b and reflects the additional pressure applied

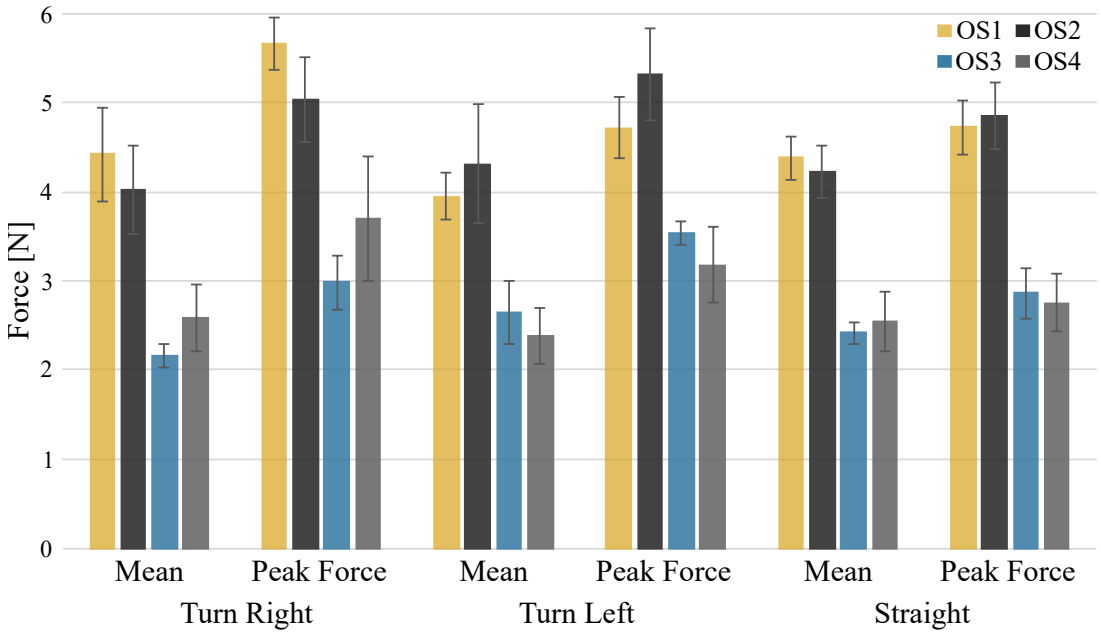

Figure 21 – Metrics obtained during the path-following tests with the SAW. Blocks represent mean values, and error bars indicate standard deviation.

to the external handlebar to stabilize the walker when changing direction. In contrast, during ST the peak forces are more balanced among all four sensors, with smaller relative differences, confirming the expected symmetry of interaction when no turning effort is required.

An additional observation is the consistent difference between upper and lower sensors. Across all conditions, the upper sensors record significantly higher amplitudes, corresponding to unloading forces applied on the top of the handlebar. In contrast, the lower sensors measure smaller values, which are mainly associated with gripping forces. This vertical differentiation demonstrates that the sensing configuration is capable not only of identifying lateral redistribution of forces during turning but also of discriminating between distinct types of user interaction, thereby providing richer information for the interpretation of locomotion strategies.

Regarding the statistical analysis, significant differences were observed in all cases when comparing the mean and peak force features extracted from the OS force signals across the path-following trajectories (i.e., during ANOVA/Friedman tests). Therefore, post-hoc pairwise comparisons were performed to identify the specific trajectory pairs for which these differences were statistically significant. Table 5 summarizes the resulting p-values obtained from the post-hoc tests.

Table 5 – Obtained p-values after pairwise comparisons using the post-hoc test. The parameters highlighted in bold were found to be statistically different.

OS	**Mean**			**Peak Force**		
	LT vs RT	**LT vs ST**	**ST vs RT**	**LT vs RT**	**LT vs ST**	**ST vs RT**
OS1	**0.01**	1.0	**<0.01**	**<0.01**	**<0.01**	0.50
OS2	**<0.01**	**0.04**	1.0	**<0.01**	0.09	**<0.01**
OS3	**<0.01**	**0.01**	**<0.01**	**0.01**	0.30	**<0.01**
OS4	**0.01**	0.70	**<0.01**	**<0.01**	**<0.01**	**<0.01**

These results indicate that LT vs RT shows statistically significant differences for all OSs, supporting the ability of the sensing system to reliably capture force redistribution during turning maneuvers. This is consistent with the trends observed in Figs. 20a–b and 21, where the sensors located on the outside handle exhibit the highest magnitudes: OS1 and OS4 dominate during right turns, whereas OS2 and OS3 dominate during left turns. Overall, the sensor profiles display a mirrored pattern across turning directions, such that sensors that dominate in one turning task present lower values in the opposite turn.

Additionally, OS1 and OS2, although they provide useful information, did not show significant differences when comparing LT and RT with ST in some cases. This outcome may also be related to OS2's lower calibration performance, which can make task-related differences harder to capture. Therefore, OS1 and OS2 should be used together, as

complementary sensors, to provide a more complete description of user–walker interaction. In addition, extracting a wider set of features may be beneficial for these sensors, as it could capture additional task-related patterns that are not reflected by these descriptors.

Finally, it is important to note that OS3 and OS4 may provide rich task-related information during the path-following trials. For OS3, the mean feature showed statistically significant differences across all trajectory pairs, indicating that this sensor consistently captures stable loading trends between LT, RT, and ST. Besides, OS4 showed statistically significant differences across all trajectory pairs for the peak force feature, suggesting higher sensitivity to variations captured in the maximum force events. This behavior in OS4 may be associated with its consistent performance during calibration.

5 Conclusions and Future Work

This dissertation presented the design, development, and validation of a novel OS for monitoring physical interaction forces in SWs. The proposed sensing approach integrates light-sensitive PDs and addressable RGB LEDs within an encapsulation material, enabling accurate estimation of applied forces while preserving a robust, and easy-to-fabricate design. Compared to conventional force-sensing technologies (such as strain gauges, capacitive sensors, and high resolution triaxial force cells), as well as optical fiber-based solutions including POFs and FBGs, the proposed sensor reduces system complexity, wiring requirements, and overall cost. These characteristics enhance its practical viability for SW applications, particularly in scenarios where compactness, scalability, and ease of integration are critical.

The results obtained for the first OS version confirm the effectiveness of the proposed sensing approach. The FNN achieved an average force estimation error of 2.4%, while the RF model classified contact zones with an accuracy of 98%, demonstrating reliable performance in both regression and classification tasks. In addition, the sensor was able to capture not only directly applied forces but also their spatial distribution across the sensing surface, suggesting its potential for future analysis of more complex interaction patterns. Some limitations were observed in the estimation of very small forces, indicating that further improvements in sensor manufacturing, calibration strategies, or model optimization could enhance performance at low load levels.

Based on these results, the second stage of this work focused on the validation of a redesigned OS with geometries better adapted to the walker handle. The new designs increased hand coverage and enabled force sensing across different interaction zones, both above and below the handle. A FNN architecture was implemented to model the relationship between the OS outputs and the applied loads. Experimental results demonstrated reliable detection of both localized and distributed forces, strong agreement with reference measurements, and consistent performance under dynamic conditions. These findings highlight the potential of the redesigned OS for seamless integration into SWs, supporting improved monitoring of user interaction while maintaining low system complexity and cost.

The comparative evaluation of encapsulation materials and LED colors with the redesigned OS revealed that the Ecoflex illuminated with red light provided the most reliable performance. This configuration achieved the lowest MSE (Validation: 4.72 ± 0.31 - Test: 4.96), MAE (Validation: 1.61 ± 0.04 - Test: 1.79), and the highest R^2 (Validation: 0.98 ± 0.01 - Test: 0.97). These results highlight the combined effect of Ecoflex's higher

deformability and the PD sensitivity in the red–near-infrared spectral range. Besides, when the best-performing sensor configuration was evaluated under new loading conditions, an average error of 5.56% was obtained, confirming its ability to generalize to unseen forces. In contrast, sensor fabricated with Clear Flex showed faster saturation and lower performance, particularly under blue illumination, underscoring the importance of material selection and wavelength choice for achieving robust sensor responses.

To further assess the repeatability and robustness of the proposed sensing approach, new four OS units were fabricated. Each sensor was calibrated using a controlled static loading procedure, and a dedicated FNN was trained per unit to account for sensor-specific variability. The results revealed consistent performance across the OSs, with OS4 achieving the best performance, showing the lowest prediction errors (MSE validation: 3.11 ± 0.55, test: 3.33; MAE validation: 1.18 ± 0.10, test: 1.24) and the highest correlation values (R^2 validation: 0.98 ± 0.02, test: 0.98). In contrast, OS2 exhibited the lowest performance, with higher MSE (Validation: 6.08 ± 0.42 - Test: 6.27, MAE (Validation: 1.73 ± 0.03 - Test: 2.15) and lower R^2 (Validation: 0.97 ± 0.03 - Test: 0.96). These differences suggest variations in PD alignment, light propagation, or material deformation introduced during fabrication. A subsequent static validation against a commercial insole-based reference system confirmed strong overall performance, with estimation errors consistently below 5.78% across all sensors.

Finally, the integration of the OSs into the SW during path-following tasks demonstrated their effectiveness in real-world environments. Across 90 trials involving straight paths and turning maneuvers, the system consistently captured force redistribution patterns, with outer sensors recording higher values during turns and upper sensors reflecting unloading forces compared to the gripping forces detected by lower sensors. This differentiation confirmed the consistency of the OSs responses, and highlighted their potential to enrich the understanding of user–walker interaction.

Building on these observations, the statistical results confirm that the system captures differences between the path-following tasks. In particular, LT and RT were significantly different for all OSs, which agrees with the mirrored force redistribution observed during turning (OS1 and OS4 higher during right turns, and OS2 and OS3 higher during left turns). OS1 and OS2 still provided useful information, but in some cases they did not show statistically significant differences relative to straight walking, which may be influenced by OS2's lower calibration performance. This suggests that OS1 and OS2 should be used together as complementary sensors, and that extracting additional features beyond mean and peak could help capture task-related patterns that are not reflected by these descriptors. In contrast, OS3 separated all trajectory pairs using the mean feature (reflecting more stable loading), while OS4 separated all pairs using the peak feature (capturing maneuver-related peaks), suggesting that each OS can provide useful

information on its own.

Future research will focus on increasing the spatial resolution of the OSs to provide richer information about the user interaction. This could be achieved by extending the sensing surface or increasing the number of PDs, enabling more detailed analysis of grip distribution and force transfer. Additional validation studies will be conducted with clinical populations, including older adults and individuals with neurological or musculoskeletal impairments, to assess sensor performance under more diverse and realistic usage conditions. Long-term evaluations will also be considered to analyze durability and signal stability over extended periods of use. From a systems perspective, future work will explore the integration of the proposed OSs into adaptive control strategies, enabling SWs to adjust assistance levels in real time based on user interaction forces. Finally, more advanced learning architectures, such as temporal or hybrid models, may be investigated to better capture nonlinear and dynamic interaction patterns during assisted walking.

Bibliography

ADOLPH, K. E. et al. How Do You Learn to Walk? Thousands of Steps and Dozens of Falls per Day. *Psychological Science*, v. 23, n. 11, p. 1387–1394, nov 2012. ISSN 0956-7976. Citado na página 21.

AERKEN, R.; CLARK, H.; BRODERICK, P. A scoping review of cane use in people who have had a stroke. *Physiotherapy Practice and Research*, SAGE Publications Sage UK: London, England, v. 45, n. 2, p. 153–167, 2024. Citado na página 23.

ALASHRAM, A. R.; ANNINO, G.; PADUA, E. Robot-assisted gait training in individuals with spinal cord injury: A systematic review for the clinical effectiveness of lokomat. *Journal of Clinical Neuroscience*, Elsevier, v. 91, p. 260–269, 2021. Citado na página 24.

ALVES, J. et al. Overview of the ASBGo++ Smart Walker. In: *2017 IEEE 5th Portuguese Meeting on Bioengineering (ENBENG)*. [S.l.]: IEEE, 2017. p. 1–4. ISBN 978-1-5090-4801-4. Citado na página 26.

AMIDEI, C. B. et al. Epidemiology of traumatic spinal cord injury: a large population-based study. *Spinal Cord*, Nature Publishing Group UK London, v. 60, n. 9, p. 812–819, 2022. Citado na página 22.

ATOYEBI, O. A. et al. Mobility challenges among older adult mobility device users. *Current Geriatrics Reports*, Springer, v. 8, n. 3, p. 223–231, 2019. Citado na página 23.

BALLESTEROS, J. et al. On gait analysis estimation errors using force sensors on a smart rollator. *Sensors*, MDPI, v. 16, n. 11, p. 1896, 2016. Citado 5 vezes nas páginas 8, 27, 28, 29, and 50.

BALLESTEROS, J. et al. Automatic assessment of a rollator-user's condition during rehabilitation using the i-walker platform. *IEEE Transactions on Neural Systems and Rehabilitation Engineering*, IEEE, v. 25, n. 11, p. 2009–2017, 2017. Citado na página 27.

BRAUN, B. J. et al. Validation and reliability testing of a new, fully integrated gait analysis insole. *Journal of foot and ankle research*, Springer, v. 8, n. 1, p. 54, 2015. Citado na página 42.

BROADWAY, C. et al. Toward commercial polymer fiber bragg grating sensors: Review and applications. *Journal of Lightwave Technology*, OSA, v. 37, n. 11, p. 2605–2615, 2019. Citado 2 vezes nas páginas 30 and 31.

BROWN, C. J.; FLOOD, K. L. Mobility limitation in the older patient: a clinical review. *Jama*, American Medical Association, v. 310, n. 11, p. 1168–1177, 2013. Citado na página 22.

BUCHMAN, A. S. et al. Cognitive function is associated with the development of mobility impairments in community-dwelling elders. *The American Journal of Geriatric Psychiatry*, Elsevier, v. 19, n. 6, p. 571–580, 2011. Citado na página 15.

BUCHMAN, A. S. et al. Cognitive Function is Associated with the Development of Mobility Impairments in Community-Dwelling Elders. *Am J Geriatr Psychiatry*, American Association for Geriatric Psychiatry, v. 19, n. 6, p. 571–580, 2011. ISSN 1064-7481. Citado na página 21.

CAETANO, I. et al. Development of a Biofeedback Approach Using Body Tracking with Active Depth Sensor in ASBGo Smart Walker. In: *2016 International Conference on Autonomous Robot Systems and Competitions (ICARSC)*. [S.l.]: IEEE, 2016. p. 241–246. ISBN 978-1-5090-2255-7. Citado na página 26.

CASAS, J. et al. Large-range polymer optical-fiber strain-gauge sensor for elastic tendons in wearable assistive robots. *Materials*, MDPI, v. 12, n. 9, p. 1443, 2019. Citado na página 30.

CHALAKI, M. et al. Vision-based fuzzy control system with intention detection for smart walkers: Enhancing usability for stroke survivors with unilateral upper limb impairments. In: IEEE. *2025 IEEE International Conference on Robotics and Automation (ICRA)*. [S.l.], 2025. p. 1997–2003. Citado 5 vezes nas páginas 8, 26, 28, 37, and 44.

CHALVATZAKI, G. G. et al. Towards an intelligent robotic walker for assisted living using multimodal sensorial data. In: IEEE. *2014 4th International Conference on Wireless Mobile Communication and Healthcare-Transforming Healthcare Through Innovations in Mobile and Wireless Technologies (MOBIHEALTH)*. [S.l.], 2014. p. 156–159. Citado na página 30.

CHAPARRO-CÁRDENAS, S. L. et al. A review in gait rehabilitation devices and applied control techniques. *Disability and Rehabilitation: Assistive Technology*, Taylor & Francis, v. 13, n. 8, p. 819–834, 2018. Citado na página 24.

CICIRELLI, G. et al. Human gait analysis in neurodegenerative diseases: A review. *IEEE journal of biomedical and health informatics*, IEEE, v. 26, n. 1, p. 229–242, 2021. Citado na página 21.

CIFUENTES, C. A.; FRIZERA, A. *Human-robot interaction strategies for walker-assisted locomotion*. [S.l.]: Springer, 2016. v. 115. Citado 2 vezes nas páginas 21 and 25.

CIFUENTES, C. A. et al. Fundamentals for the design of smart walkers. *Interfacing Humans and Robots for Gait Assistance and Rehabilitation*, Springer, p. 121–141, 2022. Citado 5 vezes nas páginas 16, 17, 23, 27, and 29.

CIFUENTES, C. A. et al. Control strategies for human–robot–environment interaction in assisted gait with smart walkers. *Interfacing Humans and Robots for Gait Assistance and Rehabilitation*, Springer, p. 259–286, 2022. Citado 2 vezes nas páginas 16 and 48.

CIFUENTES, C. A.; MúNERA, M. *Interfacing Humans and Robots for Gait Assistance and Rehabilitation*. 1. ed. [S.l.]: Springer International Publishing, 2022. v. 1. ISBN 978-3-030-79629-7. Citado 4 vezes nas páginas 15, 23, 24, and 29.

CORTÉS, U. et al. A share-it service to elders' mobility using the i-walker. *Gerontechnology*, v. 7, n. 2, p. 95, 2008. Citado na página 27.

COWAN, R. E. et al. Recent trends in assistive technology for mobility. *Journal of neuroengineering and rehabilitation*, Springer, v. 9, n. 1, p. 20, 2012. Citado na página 23.

DECKER, L. M.; CIGNETTI, F.; STERGIOU, N. Complexity and Human Gait. *Revista Andaluza de Medicina del Deporte*, v. 3, n. 1, p. 2–12, 2010. ISSN 18887546. Citado na página 21.

DÍAZ, C. A. et al. A cost-effective edge-filter based fbg interrogator using catastrophic fuse effect micro-cavity interferometers. *Measurement*, Elsevier, v. 124, p. 486–493, 2018. Citado 2 vezes nas páginas 17 and 31.

DIAZ, C. A. R. et al. Perrogator: A portable energy-efficient interrogator for dynamic monitoring of wavelength-based sensors in wearable applications. *Sensors*, MDPI, v. 19, n. 13, p. 2962, 2019. Citado 2 vezes nas páginas 17 and 31.

DING, D.-M. et al. Fall detection system on smart walker based on multisensor data fusion and sprt method. *IEEE Access*, IEEE, v. 10, p. 80932–80948, 2022. Citado 3 vezes nas páginas 17, 28, and 29.

ECKSTROM, E. et al. Physical activity and healthy aging. *Clinics in geriatric medicine*, Elsevier, v. 36, n. 4, p. 671–683, 2020. Citado 2 vezes nas páginas 15 and 22.

EFTHIMIOU, E.; FOTINEA, S. E.; GOULAS, T. The MOBOT rollator human-robot interaction model and user evaluation process. *2016 IEEE Symposium Series on Computational Intelligence, SSCI 2016*, 2017. Citado na página 26.

EL-AZIZI, A. et al. Compact led-based displacement sensing for robot fingers. *arXiv preprint arXiv:2410.03481*, 2024. Citado na página 31.

ELANGOVAN, R.; CHANDRAKUMAR, T.; SAKTHIPRIYA, D. Exploring opportunities and challenges of smart walkers for elderly users: A survey. *IEEE Pervasive Computing*, IEEE, 2025. Citado 5 vezes nas páginas 15, 17, 24, 25, and 28.

FEIGIN, V.; KRISHNAMURTHI, R. Epidemiology of Stroke. In: NORRVING, B. (Ed.). *Oxford Textbook of Sroke and Cerebrovascular Disorders*. 1. ed. New York: Oxford University Press, 2014. cap. 1, p. 1 – 8. Citado na página 22.

FEIGIN, V. L. et al. World stroke organization: global stroke fact sheet 2025. *International Journal of Stroke*, SAGE Publications Sage UK: London, England, v. 20, n. 2, p. 132–144, 2025. Citado 2 vezes nas páginas 21 and 22.

FERRARI, F. et al. Human–robot interaction analysis for a smart walker for elderly: The acanto interactive guidance system. *International Journal of Social Robotics*, Springer, v. 12, n. 2, p. 479–492, 2020. Citado na página 26.

FRANK, G. et al. The effects of silicone enclosure colour on the function of optical sensors. *Biology*, MDPI, v. 11, n. 6, p. 932, 2022. Citado na página 50.

FRIZERA-NETO, A. et al. Smart Walkers : Advanced Robotic Human Walking-Aid Systems. In: *Springer Tracts in Advanced Robotics 106 Intelligent Assistive Robots Recent Advances in Assistive Robotics*. [S.l.]: Springer International Publishing, 2015. cap. Smart Walk, p. 103 – 131. ISBN 9783319129228. Citado 3 vezes nas páginas 8, 25, and 26.

FRIZERA-NETO, A. et al. Smart walkers: Advanced robotic human walking-aid systems. In: *Intelligent Assistive Robots: Recent Advances in Assistive Robotics for Everyday Activities*. [S.l.]: Springer, 2015. p. 103–131. Citado na página 25.

GARCIA, D. et al. Semi-remote gait assistance interface: a joystick with visual feedback capabilities for therapists. *Sensors*, MDPI, v. 21, n. 10, p. 3521, 2021. Citado na página 23.

GARCIA, D. et al. Development of an optical technology-based sensor and deep learning models to estimate user-interaction forces in smart walkers. In: SPIE. *Biophotonics in Exercise Science, Sports Medicine, Health Monitoring Technologies, and Wearables VI*. [S.l.], 2025. v. 13313, p. 43–49. Citado na página 30.

GARROTE, L. et al. Robot-Assisted Navigation for a Robotic Walker with Aided User Intent. *RO-MAN 2018 - 27th IEEE International Symposium on Robot and Human Interactive Communication*, p. 348–355, 2018. Citado na página 26.

GERAVAND, M. et al. An Integrated Decision Making Approach for Adaptive Shared Control of Mobility Assistance Robots. *International Journal of Social Robotics*, Springer Netherlands, v. 8, n. 5, p. 631–648, 2016. ISSN 18754805. Citado 3 vezes nas páginas 8, 25, and 26.

GERAVAND, M. et al. An integrated decision making approach for adaptive shared control of mobility assistance robots. *International Journal of Social Robotics*, Springer, v. 8, n. 5, p. 631–648, 2016. Citado na página 30.

GHENO, R. et al. Musculoskeletal disorders in the elderly. *Journal of clinical imaging science*, v. 2, p. 39, 2012. Citado na página 15.

GONÇALVES, C. et al. Deep learning-based approaches for human motion decoding in smart walkers for rehabilitation. *Expert Systems with Applications*, Elsevier, v. 228, p. 120288, 2023. Citado 2 vezes nas páginas 8 and 25.

HU, X. et al. Spinal cord injury: molecular mechanisms and therapeutic interventions. *Signal transduction and targeted therapy*, Nature Publishing Group UK London, v. 8, n. 1, p. 245, 2023. Citado na página 22.

HUANG, C. et al. Shared navigational control and user intent detection in an intelligent walker. *AAAI Fall 2005*, 2005. Citado na página 27.

HUANG, J. et al. Proxy-based control of intelligent assistive walker for intentional sit-to-stand transfer. *IEEE/ASME Transactions on Mechatronics*, IEEE, v. 27, n. 2, p. 904–915, 2021. Citado 2 vezes nas páginas 29 and 30.

ITADERA, S.; CHENG, G. In-hand admittance controller for a robotic assistive walker based on tactile grasping feedback. *IEEE Robotics and Automation Letters*, IEEE, v. 7, n. 4, p. 8845–8852, 2022. Citado 4 vezes nas páginas 8, 28, 29, and 37.

JIMENEZ, M. F. et al. Multimodal interaction strategies for walker-assisted gait: A case study for rehabilitation in post-stroke patients. *Journal of Intelligent & Robotic Systems*, Springer, v. 110, n. 1, p. 13, 2024. Citado na página 48.

JIMÉNEZ, M. F. et al. Admittance Controller with Spatial Modulation for Assisted Locomotion using a Smart Walker. *Journal of Intelligent & Robotic Systems*, p. 1, jul 2018. ISSN 0921-0296. Citado na página 26.

JOHNSON, C. O.; NGUYEN, M. Global, regional, and national burden of stroke, 1990–2016: a systematic analysis for the Global Burden of Disease Study 2016. *The Lancet Neurology*, v. 18, n. 5, p. 439–458, may 2019. ISSN 14744422. Citado na página 21.

JOHNSON, W. et al. Stroke: a global response is needed. *Bulletin of the World Health Organization*, v. 94, n. 9, p. 634–634A, sep 2016. ISSN 0042-9686. Citado 2 vezes nas páginas 21 and 22.

KAPSALIS, E.; JAEGER, N.; HALE, J. Disabled-by-design: effects of inaccessible urban public spaces on users of mobility assistive devices–a systematic review. *Disability and Rehabilitation: Assistive Technology*, Taylor & Francis, v. 19, n. 3, p. 604–622, 2024. Citado 2 vezes nas páginas 15 and 23.

KONSTANTINOVA, J.; STILLI, A.; ALTHOEFER, K. Fingertip fiber optical tactile array with two-level spring structure. *Sensors*, MDPI, v. 17, n. 10, p. 2337, 2017. Citado 4 vezes nas páginas 17, 31, 34, and 51.

LACEY, G. J.; RODRIGUEZ-LOSADA, D. The evolution of guido. *IEEE Robotics and Automation Magazine*, v. 15, n. 4, p. 75–83, 2008. ISSN 10709932. Citado 2 vezes nas páginas 8 and 25.

LACÔTE, I. et al. Do vibrotactile patterns on both hands improve guided navigation with a walker? In: SPRINGER. *International Conference on Human Haptic Sensing and Touch Enabled Computer Applications*. [S.l.], 2024. p. 391–404. Citado na página 37.

LEAL-JUNIOR, A.; ANDRADE, R. M. de; FILHO, A. B. Series elastic actuator: Design, analysis and comparison. *Recent Advances in Robotic Systems*, InTech Rijeka, Croatia, v. 1, n. 3, 2016. Citado na página 17.

LEAL-JUNIOR, A.; NEDOMA, J.; MARTINEK, R. The role of photonic sensing technologies in healthcare 5.0: a comprehensive review of future perspectives and applications. *IEEE Internet of Things Journal*, IEEE, 2025. Citado na página 30.

LEAL-JUNIOR, A. et al. Fiber bragg gratings in cytop fibers embedded in a 3d-printed flexible support for assessment of human–robot interaction forces. *Materials*, MDPI, v. 11, n. 11, p. 2305, 2018. Citado na página 17.

LEAL-JUNIOR, A. G. et al. Polymer optical fiber sensors in healthcare applications: A comprehensive review. *Sensors*, MDPI, v. 19, n. 14, p. 3156, 2019. Citado 4 vezes nas páginas 17, 18, 30, and 31.

LEAL-JUNIOR, A. G. et al. 3d-printed pof insole: Development and applications of a low-cost, highly customizable device for plantar pressure and ground reaction forces monitoring. *Optics & Laser Technology*, Elsevier, v. 116, p. 256–264, 2019. Citado na página 17.

LEAL-JUNIOR, A. G. et al. Polymer optical fiber strain gauge for human-robot interaction forces assessment on an active knee orthosis. *Optical Fiber Technology*, Elsevier, v. 41, p. 205–211, 2018. Citado 2 vezes nas páginas 17 and 30.

LEAL-JUNIOR, A. G. et al. Plane-by-plane written, low-loss polymer optical fiber bragg grating arrays for multiparameter sensing in a smart walker. *IEEE Sensors Journal*, IEEE, v. 19, n. 20, p. 9221–9228, 2019. Citado 3 vezes nas páginas 17, 31, and 57.

LEE, G. et al. JAIST Robotic Walker control based on a two-layered Kalman filter. *Proceedings - IEEE International Conference on Robotics and Automation*, p. 3682–3687, 2011. ISSN 10504729. Citado na página 25.

LEE, G.; OHNUMA, T.; CHONG, N. Y. Design and control of JAIST active robotic walker. *Intelligent Service Robotics*, v. 3, n. 3, p. 125–135, 2010. ISSN 18612776. Citado na página 25.

LEE, H. et al. Comparative study on overground gait of stroke survivors with a conventional cane and a haptic cane. *IEEE transactions on neural systems and rehabilitation engineering*, IEEE, v. 29, p. 2183–2192, 2021. Citado na página 23.

LEVI, A. et al. Soft, transparent, electronic skin for distributed and multiple pressure sensing. *Sensors*, Molecular Diversity Preservation International (MDPI), v. 13, n. 5, p. 6578–6604, 2013. Citado 2 vezes nas páginas 17 and 31.

LI, T. et al. A fingertip optical fiber composite sensor with conformal design for robotic perception of tactile force. *IEEE/ASME Transactions on Mechatronics*, IEEE, 2024. Citado 3 vezes nas páginas 35, 36, and 48.

LIN, Y.-H. et al. Development of high-performance optical silicone for the packaging of high-power leds. *IEEE Transactions on Components and Packaging Technologies*, IEEE, v. 33, n. 4, p. 761–766, 2010. Citado na página 49.

LU, C.-K.; HUANG, Y.-C.; LEE, C.-J. Adaptive guidance system design for the assistive robotic walker. *Neurocomputing*, Elsevier, v. 170, p. 152–160, 2015. Citado 2 vezes nas páginas 28 and 29.

LU, Y. et al. Global incidence and characteristics of spinal cord injury since 2000–2021: a systematic review and meta-analysis. *BMC medicine*, Springer, v. 22, n. 1, p. 285, 2024. Citado na página 22.

MACHADO, F. et al. Virtual obstacle avoidance strategy: Navigating through a complex environment while interacting with virtual and physical elements. *Sensors (Basel, Switzerland)*, v. 24, n. 19, p. 6212, 2024. Citado 2 vezes nas páginas 8 and 25.

MACHADO, F. et al. A novel mixed reality assistive system to aid the visually and mobility impaired using a multimodal feedback system. *Displays*, Elsevier, v. 79, p. 102480, 2023. Citado 2 vezes nas páginas 26 and 28.

MARTINS, M. et al. A review of the functionalities of smart walkers. *Medical engineering & physics*, Elsevier, v. 37, n. 10, p. 917–928, 2015. Citado 7 vezes nas páginas 15, 17, 23, 24, 27, 28, and 29.

MARTINS, M. et al. Design, implementation and testing of a new user interface for a smart walker. In: *2014 IEEE International Conference on Autonomous Robot Systems and Competitions (ICARSC)*. [S.l.]: IEEE, 2014. p. 217–222. ISBN 978-1-4799-4254-1. Citado na página 26.

MARTINS, M. M. et al. Assistive mobility devices focusing on smart walkers: Classification and review. *Robotics and Autonomous Systems*, Elsevier, v. 60, n. 4, p. 548–562, 2012. Citado na página 25.

Mayo Clinic. *Spinal cord injury*. 2019. Disponível em: <https://www.mayoclinic.org/diseases-conditions/spinal-cord-injury/symptoms-causes/syc-20377890>. Citado na página 22.

MENEGARDO, R.; LEAL-JUNIOR, A. Multiplexing technique using photodetector arrays for quasi-distributed intensity variation optical fiber sensors system. *Optics & Laser Technology*, Elsevier, v. 188, p. 112883, 2025. Citado 2 vezes nas páginas 51 and 55.

Microchip Technology Inc. *MCP6021/1R/2/3/4: Rail-to-Rail Input/Output, 10 MHz Op Amps*. [S.l.], 2017. Datasheet. Citado na página 34.

MIKOLAJCZYK, T. et al. Advanced technology for gait rehabilitation: An overview. *Advances in Mechanical Engineering*, SAGE Publications Sage UK: London, England, v. 10, n. 7, p. 1687814018783627, 2018. Citado 2 vezes nas páginas 15 and 22.

Mimi Poinsett, P. Cerebral Palsy Prevalence and Incidence. *Cerebral Palsy Guidance*, oct 2019. Disponível em: <https://www.cerebralpalsyguidance.com/cerebral-palsy/research/prevalence-and-incidence/>. Citado na página 22.

MORENO, J. et al. Wearable robot technologies. *Wearable robots: biomechatronic exoskeletons.*, p. 165–99, 2008. Citado na página 30.

MORRIS, A. et al. A robotic walker that provides guidance. *2003 IEEE International Conference on Robotics and Automation (Cat. No.03CH37422)*, v. 1, p. 25–30, 2003. ISSN 1050-4729. Citado na página 25.

MOU, W.-H. et al. Context-aware assisted interactive robotic walker for Parkinson's disease patients. In: *2012 IEEE/RSJ International Conference on Intelligent Robots and Systems*. [S.l.]: IEEE, 2012. p. 329–334. ISBN 978-1-4673-1736-8. ISSN 21530858. Citado na página 25.

NABILI, S. N.; DAVIS, C. P. *Senior Health: Successful Aging*. 2019. Citado na página 22.

NADERER, M. et al. Development and control of a robotic assistant walking aid for fall risk reduction. *Frontiers in Robotics and AI*, Frontiers Media SA, v. 12, p. 1646803, 2025. Citado na página 26.

NGIEJUNGBWEN, L. A.; HAMDAOUI, H.; CHEN, M.-Y. Polymer optical fiber and fiber bragg grating sensors for biomedical engineering applications: A comprehensive review. *Optics & Laser Technology*, Elsevier, v. 170, p. 110187, 2024. Citado na página 30.

OHNUMA, T.; LEE, G.; CHONG, N. Y. Particle filter based feedback control of jaist active robotic walker. In: IEEE. *2011 RO-MAN*. [S.l.], 2011. p. 264–269. Citado 2 vezes nas páginas 8 and 25.

PALOPOLI, L.; ARGYROS, A.; BIRCHBAUER, J. Navigation assistance and guidance of older adults across complex public spaces : the DALi approach. *Intel Serv Robotics*, p. 77–92, 2015. Citado na página 27.

PAPAGEORGIOU, X. S. et al. Experimental validation of human pathological gait analysis for an assisted living intelligent robotic walker. *Proceedings of the IEEE RAS and EMBS International Conference on Biomedical Robotics and Biomechatronics*, v. 2016-July, p. 1086–1091, 2016. ISSN 21551774. Citado na página 26.

PATEL, R.; CORRELL, N. Integrated force and distance sensing using elastomer-embedded commodity proximity sensors. In: *Robotics: Science and systems*. [S.l.: s.n.], 2016. Citado na página 31.

PAUL, S. et al. A review on recent advances of cerebral palsy. *Oxidative medicine and cellular longevity*, Wiley Online Library, v. 2022, n. 1, p. 2622310, 2022. Citado na página 22.

PAULO, J.; PEIXOTO, P.; NUNES, U. J. ISR-AIWALKER: Robotic Walker for Intuitive and Safe Mobility Assistance and Gait Analysis. *IEEE Transactions on Human-Machine Systems*, v. 47, n. 6, p. 1110–1122, 2017. ISSN 21682291. Citado na página 26.

PETERS, K. Polymer optical fiber sensors—a review. *Smart materials and structures*, IOP Publishing, v. 20, n. 1, p. 013002, 2010. Citado na página 17.

PHAM, D. D.; DUONG, H. T.; SUH, Y. S. Walking monitoring for users of standard and front-wheel walkers. *IEEE Transactions on Instrumentation and Measurement*, IEEE, v. 66, n. 12, p. 3289–3298, 2017. Citado na página 24.

PIACENZA, P. et al. A sensorized multicurved robot finger with data-driven touch sensing via overlapping light signals. *IEEE/ASME Transactions on Mechatronics*, IEEE, v. 25, n. 5, p. 2416–2427, 2020. Citado 10 vezes nas páginas 18, 31, 33, 35, 36, 39, 48, 50, 51, and 54.

PIRKER, W.; KATZENSCHLAGER, R. Gait disorders in adults and the elderly. *Wiener klinische Wochenschrift*, v. 129, n. 3-4, p. 81–95, feb 2017. ISSN 0043-5325. Citado na página 22.

POSTOLACHE, O. et al. Smart walker solutions for physical rehabilitation. *IEEE Instrumentation & Measurement Magazine*, IEEE, v. 18, n. 5, p. 21–30, 2015. Citado na página 24.

RASOULI, F.; REED, K. B. Walking assistance using crutches: A state of the art review. *Journal of Biomechanics*, Elsevier, v. 98, p. 109489, 2020. Citado na página 23.

REICH, M. et al. Pof force sensor for human-robot interaction strategies in robotic walker assisted gait. In: OPTICA PUBLISHING GROUP. *Optical Fiber Sensors*. [S.l.], 2022. p. W4–76. Citado na página 30.

REICH, M.; FRIZERA, A.; DÍAZ, C. A. Approximate modelling based on genetic algorithm for a pof force sensor for human-robot interaction in robotic walker. In: IEEE. *2022 IEEE Latin American Electron Devices Conference (LAEDC)*. [S.l.], 2022. p. 1–4. Citado na página 31.

RESCH, S. et al. Smart walking aids with sensor technology for gait support and health monitoring: a scoping review. *Technologies*, MDPI, v. 13, n. 8, p. 346, 2025. Citado 3 vezes nas páginas 16, 28, and 30.

RICHARDS, C. L.; MALOUIN, F. Cerebral palsy. In: *Handbook of Clinical Neurology*. [S.l.]: Elsevier B.V., 2013. v. 111, p. 183–195. Citado na página 22.

ROHOR, P. et al. Effects of smart walker-assisted gait in real-world vs. virtual reality on heart rate variability and blood pressure in elderly: A randomized cross-over study. *Journal of Bodywork and Movement Therapies*, Elsevier, v. 45, p. 319–331, 2025. Citado 2 vezes nas páginas 22 and 30.

SCHMITT, A. C. et al. Walking indoors, outdoors, and on a treadmill: Gait differences in healthy young and older adults. *Gait & posture*, Elsevier, v. 90, p. 468–474, 2021. Citado na página 24.

SIERRA, S. et al. Assessment of a robotic walker in older adults with parkinson's disease in daily living activities. *Frontiers in neurorobotics*, Frontiers Media SA, v. 15, p. 742281, 2021. Citado na página 21.

SIERRA, S. et al. Human–robot–environment interaction interface for smart walker assisted gait: Agora walker. *Sensors*, MDPI, v. 19, n. 13, p. 2897, 2019. Citado 7 vezes nas páginas 8, 15, 24, 25, 26, 28, and 30.

SIERRA, S. et al. Socially assistive walker for daily living assistance in older adults. *Frontiers in Robotics and AI*, Frontiers Media SA, v. 11, p. 1401663, 2024. Citado 8 vezes nas páginas 8, 15, 17, 26, 27, 29, 37, and 42.

SIERRA, S. et al. Evaluation of physical interaction during walker-assisted gait with the agora walker: Strategies based on virtual mechanical stiffness. *Sensors*, MDPI, v. 21, n. 9, p. 3242, 2021. Citado 3 vezes nas páginas 17, 28, and 56.

SPENKO, M.; YU, H.; DUBOWSKY, S. Robotic personal aids for mobility and monitoring for the elderly. *IEEE Transactions on Neural Systems and Rehabilitation Engineering*, v. 14, n. 3, p. 344–351, 2006. ISSN 15344320. Citado na página 25.

STAVSKY, M. et al. Cerebral Palsy—Trends in Epidemiology and Recent Development in Prenatal Mechanisms of Disease, Treatment, and Prevention. *Frontiers in Pediatrics*, v. 5, feb 2017. ISSN 2296-2360. Citado na página 22.

TAVARES, C. et al. Optically instrumented insole for gait plantar and shear force monitoring. *IEEE Access*, IEEE, v. 9, p. 132480–132490, 2021. Citado na página 30.

TODHUNTER-BROWN, A. et al. Physical rehabilitation approaches for the recovery of function and mobility following stroke. *Cochrane Database of Systematic Reviews*, John Wiley & Sons, Ltd, n. 2, 2025. Citado 2 vezes nas páginas 15 and 23.

United Nations, Department of Economic and Social Affairs. *World population ageing 2019*. [S.l.], 2020. Citado 2 vezes nas páginas 15 and 22.

VAUGHAN, C. L. Theories of bipedal walking: an odyssey. *Journal of biomechanics*, Elsevier, v. 36, n. 4, p. 513–523, 2003. Citado 2 vezes nas páginas 15 and 21.

VAUGHAN, C. L. Theories of bipedal walking: an odyssey. *Journal of Biomechanics*, v. 36, n. 4, p. 513–523, apr 2003. ISSN 00219290. Citado na página 21.

VERDEZOTO, G.; BALLESTEROS, J.; URDIALES, C. Smart rollators aid devices: Current trends and challenges. *IEEE Transactions on Human-Machine Systems*, IEEE, v. 52, n. 6, p. 1103–1110, 2022. Citado 3 vezes nas páginas 16, 26, and 28.

VITRIKAS, K.; DALTON, H.; BREISH, D. Cerebral palsy: an overview. *American family physician*, v. 101, n. 4, p. 213–220, 2020. Citado na página 22.

WANG, Y. et al. Multimodal haptic interface for walker-assisted navigation. In: IEEE. *2024 IEEE/RSJ International Conference on Intelligent Robots and Systems (IROS)*. [S.l.], 2024. p. 141–146. Citado 4 vezes nas páginas 8, 28, 37, and 44.

World Health Organization. *Wheelchair provision guidelines*. [S.l.: s.n.], 2023. Citado na página 24.

World Health Organization. *Assistive technology*. 2024. Https://www.who.int/news-room/fact-sheets/detail/assistive-technology. Citado na página 23.

World Health Organization. *Spinal cord injury*. 2024. Accessed: Nov. 2025. Disponível em: <https://www.who.int/news-room/fact-sheets/detail/spinal-cord-injury>. Citado na página 22.

World Health Organization. *Stroke, Cerebrovascular accident*. 2024. <https://www.emro.who.int/health-topics/stroke-cerebrovascular-accident/>. Accessed: Oct. 2025. Citado na página 21.

World Health Organization. *Ageing and health*. 2025. <https://www.who.int/news-room/fact-sheets/detail/ageing-and-health>. Accessed: Oct. 2025. Citado 3 vezes nas páginas 15, 22, and 23.

XIE, L. et al. Recent advances in flexible materials for wearable optical biosensors. *Biosensors*, MDPI, v. 15, n. 9, p. 611, 2025. Citado 2 vezes nas páginas 49 and 50.

XU, W. et al. Reinforcement learning-based shared control for walking-aid robot and its experimental verification. *Advanced Robotics*, Taylor & Francis, v. 29, n. 22, p. 1463–1481, 2015. Citado 3 vezes nas páginas 8, 28, and 29.

YANG, R. et al. Epidemiology of Spinal Cord Injuries and Risk Factors for Complete Injuries in Guangdong, China: A Retrospective Study. *PLoS ONE*, v. 9, n. 1, p. e84733, jan 2014. ISSN 1932-6203. Citado na página 22.

ZOU, L. et al. Novel tactile sensor technology and smart tactile sensing systems: A review. *Sensors*, MDPI, v. 17, n. 11, p. 2653, 2017. Citado 5 vezes nas páginas 16, 17, 28, 29, and 30.